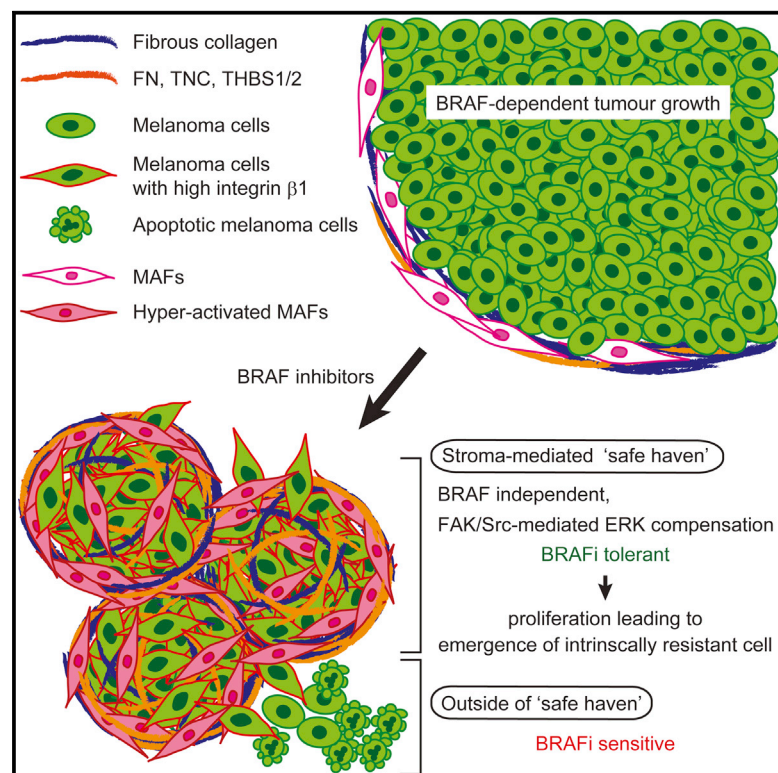Article

Intravital Imaging Reveals How BRAF Inhibition Generates Drug-Tolerant Microenvironments with High Integrin β1/FAK Signaling

Graphical Abstract

Authors

Eishu Hirata, Maria Romina Girotti, ..., Richard Marais, Erik Sahai

Correspondence

erik.sahai@crick.ac.uk

In Brief

Hirata et al. show that the BRAF inhibitor PLX4720 promotes melanoma-associated fibroblasts in *BRAF*-mutant melanomas to produce and remodel matrix, leading to integrin β1-FAK-Src signaling and reactivation of ERK and MAPK in melanoma cells. Co-inhibition of BRAF and FAK blocks ERK reactivation.

Highlights

- BRAF mutant melanoma cells respond to PLX4720 heterogeneously in vivo

- BRAF inhibition activates MAFs, leading to FAK-dependent melanoma survival signaling

- ECM-derived signals can support residual disease

- BRAF and FAK inhibition synergize in pre-clinical models

Accession Numbers

GSE63160

CrossMark

CellPress

CellPress

Intravital Imaging Reveals How BRAF Inhibition Generates Drug-Tolerant Microenvironments with High Integrin β1/FAK Signaling

Eishu Hirata,[1] Maria Romina Girotti,[2] Amaya Viros,[2] Steven Hooper,[1] Bradley Spencer-Dene,[3] Michiyuki Matsuda,[4] James Larkin,[5] Richard Marais,[2] and Erik Sahai[1,*]

[1]Tumor Cell Biology Laboratory, Cancer Research UK London Research Institute, London WC2A 3LY, UK
[2]Molecular Oncology Group, Cancer Research UK Manchester Institute, Wilmslow Road, Manchester M20 4BX, UK
[3]Experimental Histopathology Laboratory, Cancer Research UK London Research Institute, London WC2A 3LY, UK
[4]Laboratory of Bioimaging and Cell Signalling, Kyoto University Graduate School of Biostudies, Kyoto 606-8315, Japan
[5]Department of Medical Oncology, Royal Marsden NHS Trust, Fulham Road, London SW3 6JJ, UK
*Correspondence: erik.sahai@crick.ac.uk
http://dx.doi.org/10.1016/j.ccell.2015.03.008
This is an open access article under the CC BY-NC-ND license (http://creativecommons.org/licenses/by-nc-nd/4.0/).

SUMMARY

Intravital imaging of BRAF-mutant melanoma cells containing an ERK/MAPK biosensor reveals how the tumor microenvironment affects response to BRAF inhibition by PLX4720. Initially, melanoma cells respond to PLX4720, but rapid reactivation of ERK/MAPK is observed in areas of high stromal density. This is linked to "paradoxical" activation of melanoma-associated fibroblasts by PLX4720 and the promotion of matrix production and remodeling leading to elevated integrin β1/FAK/Src signaling in melanoma cells. Fibronectin-rich matrices with 3–12 kPa elastic modulus are sufficient to provide PLX4720 tolerance. Co-inhibition of BRAF and FAK abolished ERK reactivation and led to more effective control of BRAF-mutant melanoma. We propose that paradoxically activated MAFs provide a "safe haven" for melanoma cells to tolerate BRAF inhibition.

INTRODUCTION

Since the discovery of oncogenes that encoded protein kinases, it has been hoped that inhibition of the relevant kinases would be an effective chemotherapeutic strategy (Shawver et al., 2002). This aspiration has become a clinical reality with the development of inhibitors against Abl tyrosine kinase (Druker et al., 2001, 2006), EGFR family kinases (Maemondo et al., 2010; Mok et al., 2009; Sordella et al., 2004), and BRAF (Chapman et al., 2011; Flaherty et al., 2010; Sosman et al., 2012). However, agents targeting either EGFR or BRAF typically show good efficacy in tumors with matching oncogenic mutations for a number of months before genetically resistant cells dominate the tumor and the therapy fails (Kobayashi et al., 2005; Nazarian et al., 2010; Poulikakos et al., 2011; Poulikakos and Rosen, 2011; Villa-

nueva et al., 2011). In the case of EGFR-mutant lung tumors, it has been shown that resistant cells may be present even before treatment and that these are at a strong selective advantage during therapy (Inukai et al., 2006; Maheswaran et al., 2008; Rosell et al., 2011; Turke et al., 2010). However, the situation in BRAF-mutant melanoma treated with BRAF inhibitors is less clear. There is significant variability in the magnitude of initial response to BRAF inhibition (Chapman et al., 2011; Sosman et al., 2012) and genetically resistant sub-clones have not been detected prior to treatment in tumors that show modest responses. It has been proposed that non-cell autonomous mechanisms involving HGF production by the tumor stroma may drive resistance (Straussman et al., 2012; Wilson et al., 2012). However, it is not clear how selective pressure would act on the genetically stable stroma to promote the emergence of resistant disease.

Significance

Many tumors show an initial response to targeted therapies before genetic resistance emerges; however, little is known about how tumor cells might tolerate therapy before genetic resistance dominates. We show how BRAF-mutant melanoma cells rapidly become tolerant to PLX4720 in areas of high stroma. We demonstrate that PLX4720 has an effect on the tumor stroma, leading to enhanced matrix remodeling. The remodeled matrix then provides signals that enable melanoma cells to tolerate PLX4720. We propose that this safe haven enhances the population of cancer cells from which genetic resistance emerges. This work highlights the need to consider the effects of targeted therapies on the tumor microenvironment.

CrossMark
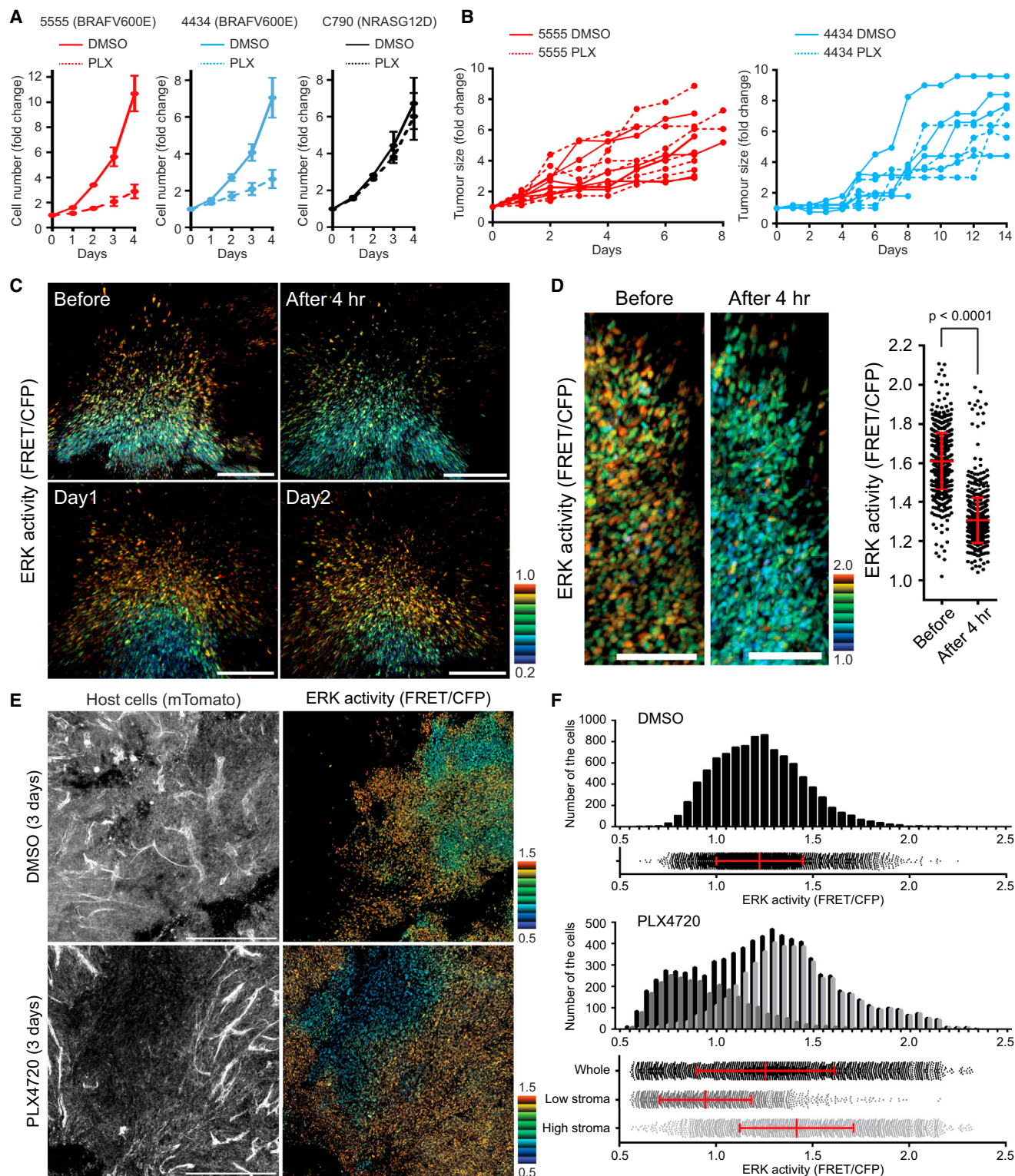
Figure 1. Melanoma Cells Respond to PLX4720 Heterogeneously In Vivo

(A and B) Growth curves of the indicated melanoma cells in vitro (A) and in vivo (B) treated with DMSO (0.1% in vitro and 4% in vivo) or PLX4720 (1 μM in vitro and 25 mg/kg in vivo). Data in (A) are represented as mean ± SD.

(C and D) Intravital longitudinal imaging of 5555-EKAREV-NLS tumors through an imaging window. The mouse was gavaged PLX4720 (25 mg/kg) every 24 hr, and images were acquired before and 4 hr after the first, second (Day 1), and third (Day 2) gavage. ERK activities in (D) were quantified and shown as mean ± SD. Scale bars represent 100 μm.

Establishing the chronology of biochemical responses to targeted therapy and biological changes elicited within the context of complex tumor microenvironments remains challenging. BRAF exerts its effects through activation of ERK/MAPK signaling. The activity of ERK/MAPK can be monitored in live tissue using a biosensor construct containing two fluorophores, a long flexible linker, an ERK/MAP kinase binding site, an optimal substrate site for the kinase, and a phospho-threonine binding domain (Harvey et al., 2008; Komatsu et al., 2011). When the substrate site is phosphorylated, it engages in an intra-molecular interaction with the phospho-threonine binding domain, leading to an overall change in the conformation of the molecule and a change in fluorescence resonance energy transfer (FRET) between the two fluorophores (Komatsu et al., 2011). This system enables the biochemical response to BRAF inhibition to be monitored with single cell resolution in vivo. Genetically engineered syngeneic hosts additionally provide the ability to depict the tumor stroma (Muzumdar et al., 2007). These technologies can be combined with intravital imaging windows to longitudinally track both the biochemical response to BRAF inhibition and the distribution of the tumor stroma (Janssen et al., 2013).

RESULTS

In Vivo Model of Extrinsic Resistance to BRAF Inhibition

To study responses to BRAF inhibition in a syngeneic tumor microenvironment, we tested the response of BRAF and NRAS mutant C57/BL6 mouse melanoma cell lines to the BRAF inhibitor PLX4720. Two different BRAF mutant lines, 5555 and 4434, were sensitive to PLX4720 whereas, as expected, the NRAS mutant cells (C790) were refractory to PLX4720 in vitro (Figure 1A). We next tested the response of these cells to PLX4720 when growing as tumors in syngeneic mice. To our surprise, both BRAF-mutant melanoma cell lines were refractory to PLX4720 (Figure 1B). This unexpected result suggested to us that these cells might represent a model to probe non-cell autonomous mechanisms of resistance of PLX4720. Furthermore, they may represent the small subset of BRAF-mutant melanoma that exhibit only a small response to vemurafenib.

To understand the lack of response of 5555 and 4434 cells to PLX4720 in vivo, we reasoned that it would be important to monitor the BRAF signaling with single cell resolution. We engineered 5555 and 4434 cells to express an ERK/MAP kinase biosensor located in the nucleus—called EKAREV-NLS (Figure S1A). The EKAREV biosensor faithfully monitored changes in ERK/MAP kinase signaling in response to TPA and either BRAF or MEK inhibitors (Figures S1B–S1E). In contrast, "paradoxical" activation of ERK/MAPK activity is observed in NRAS mutant cells treated with PLX4720 (Figures S1C and S1F). We further confirmed that changes in FRET signal are absolutely dependent upon the phospho-acceptor site in the biosensor (Figures S1G and S1H).

We next generated tumors using 5555-EKAREV-NLS cells; in some cases, these were adjacent to titanium imaging windows that allow longitudinal imaging of the same tumor (Janssen et al., 2013). Intravital imaging revealed considerable heterogeneity in EKAREV FRET signal (Figures 1C–1F, S1I, and S1J). These data are supported by ppERK immunohistochemical analysis (Figure S1K). To gain insight into the lack of effect of PLX4720 on tumor growth, we performed longitudinal imaging of tumors before and during PLX4720 treatment. The results showed that the high EKAREV FRET signal was reduced 4 hr after administration of PLX4720 (Figures 1C and 1D). These data suggest that PLX4720 can access the tumor and achieve the reduction in ERK/MAPK activity expected based on the in vitro analysis in Figures S1C–S1E. However, within 1 day, high levels of EKAREV FRET signal returned even though PLX4720 was administered daily (Figure 1C). Analysis of the distribution of EKAREV signal after 3 days of PLX4720 treatment suggested that only a small proportion of 5555 cells show a stable reduction in ERK/MAPK activity (Figures 1E and 1F). These cells were typically located in regions with low levels of host cells, which were demonstrated based on of their expression of the mTomato transgene. To more robustly test this observation, we segmented images of PLX4720 treated tumors into regions with high or low levels of mTomato signal (Figure S1L). Figure 1F shows that regions with low levels of stromal cells had significantly lower levels EKAREV FRET signal (similar data were obtained in 4434 tumors; Figure S1M). These data demonstrate BRAF mutant 5555 and 4434 tumors show a short-lived biochemical response to PLX4720. Further, the rapid re-activation of ERK/MAPK and adaptation of these tumors to PLX4720 is correlated with stromal density.

Melanoma-Associated Fibroblasts Are Sufficient to Confer Tolerance to BRAF Inhibition

We sought to establish a culture system that re-capitulated the PLX4720 tolerance that we observed in vivo. The behavior of pure spheroids of melanoma cells was compared with that of equivalent sized tumor pieces when embedded in a collagen matrix. Figures 2A and 2B show that pure melanoma spheroids were highly sensitive to PLX4720, with the appearance of many nuclear fragments indicating cell death. In contrast, melanoma explants from either subcutaneous tumors or experimentally established lung metastases were unresponsive to PLX4720 (Figures 2A and 2B). Even in the presence of drug, melanoma cells retained healthy nuclear architecture and invasive capability. Thus, the spheroid model recapitulates the stroma-dependent PLX4720 tolerance observed in vivo. It also formally excludes any problems relating to drug access that might confound interpretation of the in vivo data.

We next sought to identify the stromal cell type that might be responsible for the adaptive behavior of 5555 and 4434 melanoma. Immunohistochemical staining of 5555 and 4434 tumors revealed low number of infiltrating lymphocytes and neutrophils,

(E) Intravital images of 5555-EKAREV-NLS subcutaneously grown in C57BL/6_ROSA26-mTmG mice. Upper and lower images are from mice treated with DMSO and PLX4720 for 3 days, respectively. Left: all host cells (Tomato). Right: ERK activity in 5555 cells. Scale bars represent 500 μm.

(F) Distribution and histogram of ERK activity in control and PLX4720-treated mice. In PLX4720-treated mice, cells are separated into two groups according to the host cell density (low and high stroma) and analyzed.

Bars in the scatterplots indicate mean ± SD. See also Figure S1.
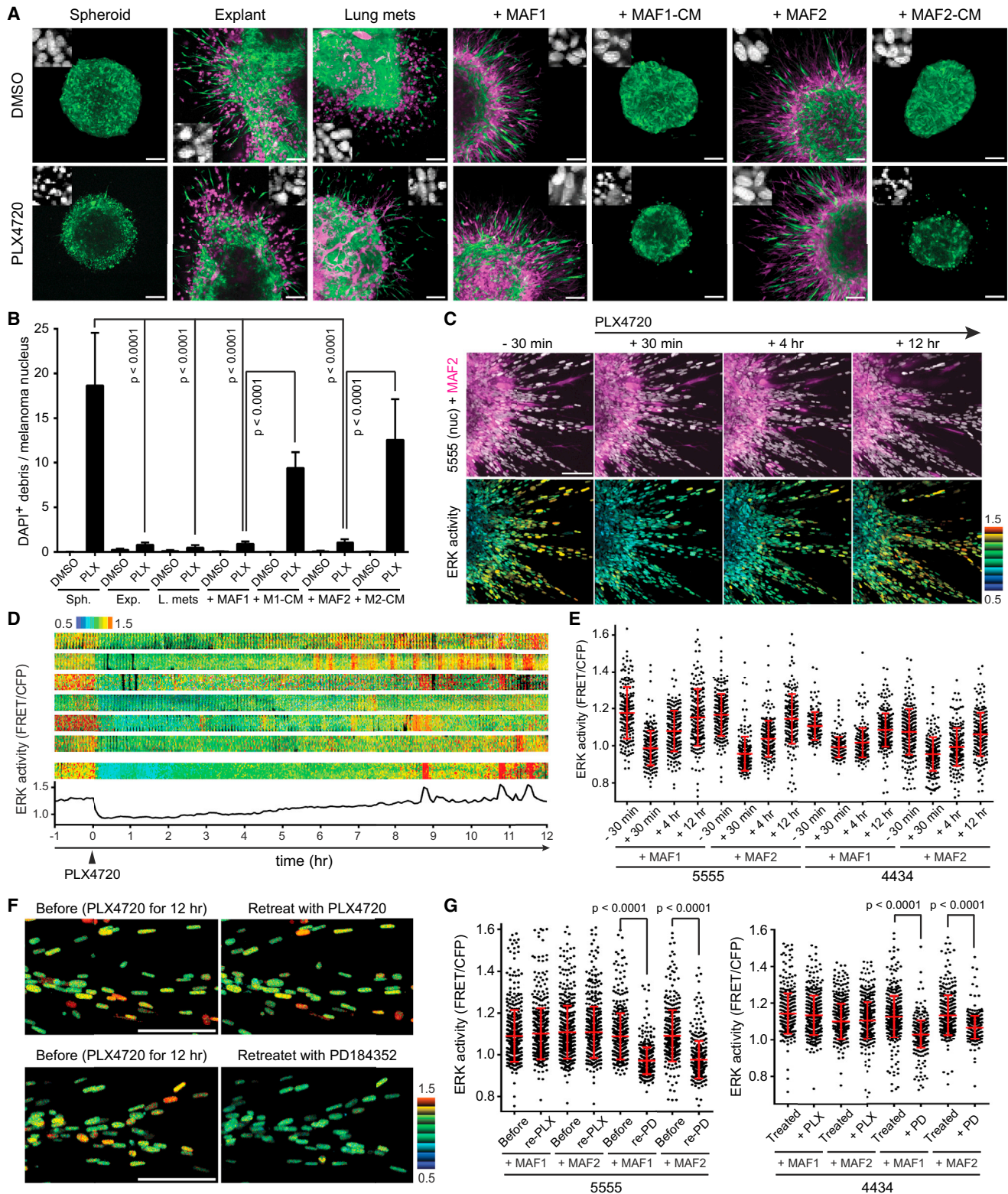
Figure 2. Stromal Cells Provide Invasive and Pro-survival Signals, and the System Adapts to the Drug Within 12 Hours

(A and B) Various types (indicated above in each panel) of 5555 melanoma spheroids/tumor explants were embedded into collagen gels and treated with 0.1% DMSO (upper panels) or 1 µM PLX4720 (lower panels) for 24 hr. 5555 cells are depicted in green, stromal cells/MAFs in magenta, and representative DAPI-stained images are also shown (A), and the ratio of DAPI-positive debris and melanoma nucleus was calculated as a cell death indicator (B). Spheroid, 5555 pure

(legend continued on next page)

and there was no clear relationship between the location of blood vessels and ppERK signals (Figure S2A). However, both macrophages and stromal fibroblasts were abundant in both DMSO- and PLX4720-treated tumors (Figure S2A). We therefore explored whether melanoma-associated fibroblasts (MAFs) or macrophages might be sufficient to confer drug tolerance on melanoma cells. Two isolates of MAFs were established from patients (designated MAF1 and MAF2, Figures S2B and S2C) and their effect on the response of 5555 and 4434 cells to PLX4720 was tested. Figures 2A, 2B, and S2D show that co-culture of either MAF1 or MAF2 with melanoma cells conferred tolerance of PLX4720 and invasive behavior. This effect was significantly dependent on close proximity of the two cell types because MAF conditioned media had only partial ability to reduce PLX4720-induced cell death (Figures 2A, 2B, S2E, and S2F). Furthermore, we excluded a role for EGFR and c-Met in mediating MAF-dependent PLX4720 tolerance (Figures S2G and S2H). Co-culture with macrophages was unable to confer drug tolerance on melanoma cells (Figure S2I). These data establish fibroblastic stromal is sufficient to confer tolerance to PLX4720.

We next investigated the activity of ERK/MAPK signaling in melanoma spheroids. FRET imaging with EKAREV-NLS shows heterogeneous ERK activity in 5555 explants and 5555/MAF co-culture spheroids (Figure S2J, and similar results with 4434 cells in Figure S2K). There was markedly reduced signal/noise of the EKAR biosensor in the explant/spheroid center; therefore, we excluded these regions from our subsequent analyses. We performed time-lapse imaging of spheroid co-cultures before and after the addition of PLX4720. Figures 2C–2E and Movie S1 reveal a marked decrease in EKAREV signal 30 min after the addition of the drug. However, within 12 hr, the EKAREV signal had returned to the level prior to drug addition. This was similar to the in vivo results. In pure melanoma spheroids, the EKAREV signal was stably decreased until cells began to die (the variable FRET signal in apoptotic cultures cannot reliably be interpreted). To exclude the possibility of drug metabolism or drug degradation, we re-added PLX4720 after 12 hr and monitored the response. Strikingly, co-cultures that had been exposed to PLX4720 for 12 hr were completely refractory to the addition of more PLX4720, while importantly, they remained sensitive to the addition of the MEK inhibitor PD184352 (Figures 2F and 2G). These data demonstrate that co-cultures of melanoma cells and MAFs switch from BRAF-dependent ERK signaling to BRAF-independent ERK signaling in just 12 hr.

PLX4720 Activates MAFs, Leading to Matrix Remodeling
The data above do not fit with existing models of drug resistance. The adaptation is too quick to be genetic and unlike the relief of

negative feedback described, the mechanism that we observe cannot be mediated by melanoma cells alone (Lito et al., 2012). We therefore hypothesized that PLX4720 might be having an effect on the tumor stroma. To test this, we engineered MAFs to contain the EKAREV-NLS biosensor and also express mCherry to enable them to be distinguished from melanoma cells. Spheroid co-cultures of 5555 and MAFs were imaged before and during the response to PLX4720. Strikingly, EKAREV FRET signal increased in MAF shortly after the addition of PLX4720 (Figures 3A–3C and S3A and Movie S2). As expected, EKAREV signal in the melanoma cells decreased immediately after the addition of the drug. ERK activation in MAFs by PLX4720 was confirmed by western blotting (Figure S3B). PLX4720 also slightly increased MAF proliferation (Figure S3C). We next tested whether PLX4720 might modulate the function of MAFs. A key feature of fibroblastic stroma is its ability to remodel the extracellular matrix (Kalluri and Zeisberg, 2006). This can be assayed using collagen gel contraction assays and imaging of collagen fibers by second harmonic generation (SHG) (Calvo et al., 2013). PLX4720 enhanced the matrix remodeling capability of both MAF1 and MAF2 and increased phosphorylation of the key regulator of actomyosin contractility, MLC2/MYL9 (Figures 3D and 3E). PLX4720 also induced dynamic protrusions in MAFs (Figure 3F and Movie S3) and promoted the formation of dense collagen fibrils (Figure 3G). In contrast to MAFs, PLX4720 did not promote significant gel contraction by normal fibroblasts (Figure S3D). This indicates that some prior level of activation is likely to be required for PLX4720 to modulate fibroblast function.

To obtain a global perspective on how PLX4720 affects MAFs, we performed microarray analysis. This revealed coordinated upregulation of the expression of many extracellular matrix (ECM) molecules in PLX4720-treated MAFs (Figures S3E and S3F; Table S1). The upregulation of thrombospondin-1 (THBS1) and tenascin-C (TNC) were confirmed using quantitative immunofluorescence (Figure 3H). In contrast, the expression of soluble growth factors previously implicated in resistance to BRAF inhibitors was largely unchanged (Figure S3E).

Interestingly, we noticed that PLX4720 increased expression of platelet-derived growth factor receptor (PDGFR) α in MAFs (Figure S3E), and previous work has shown that stromal fibroblasts are dependent on PDGFR signaling (Erez et al., 2010; Kalluri and Zeisberg, 2006; Pietras et al., 2008). We hypothesized that PLX4720 might activate MAFs by enhancing the activity of PDGFRα- and Ras-dependent signaling through the "paradoxical" activation of CRAF (Hatzivassiliou et al., 2010; Heidorn et al., 2010; Nazarian et al., 2010; Poulikakos et al., 2010; Villanueva et al., 2010). Therefore, we investigated the effect of inhibiting

---

spheroids made in vitro; explant, tumor explants of 5555 grown subcutaneously in C57BL/6_ROSA26-mTmG mice; lung mets, tumor explants of experimentally-induced lung metastasis of 5555 in C57BL/6_ROSA26-mTmG mice; +MAF1/2, 5555 and MAF co-culture spheroid made in vitro; +MAF1/2-CM, 5555 spheroids made in vitro were treated with conditioned media from MAFs. Data in (B) are represented as mean ± SD. Scale bars represent 100 μm.
(C–E) 5555/4434-EKAREV-NLS and MAF1/2-mCherry co-cultured spheroids were embedded in collagen gels and treated with PLX4720 (1 μM) at time = 0. Upper images in (C) indicate 5555 nuclei (gray) and MAF2 (magenta), and lower images indicate ERK activity (FRET/CFP) in 5555 cells. Kymographs of ERK activity in seven representative cells are shown in (D), and ERK activities at time −30 min, +30 min, +4 hr, and +12 hr are quantified and shown in (E) as scatterplots with mean ± SD. Scale bar represents 100 μm.
(F and G) 5555/4434-EKAREV-NLS and MAF1/2 co-cultured spheroids in collagen gels were treated with PLX4720 (1 μM) for 12 hr, followed by re-treatment with PLX4720 (1 μM) or PD184352 (1 μM). Representative images of 5555 co-cultured with MAF1 are shown in (F) and ERK activities (FRET/CFP) in 5555 and 4434 before and after re-treatment were quantified and shown as scatterplots with mean ± SD in (G).
Scale bars represent 100 μm. See also Figure S2 and Movie S1.
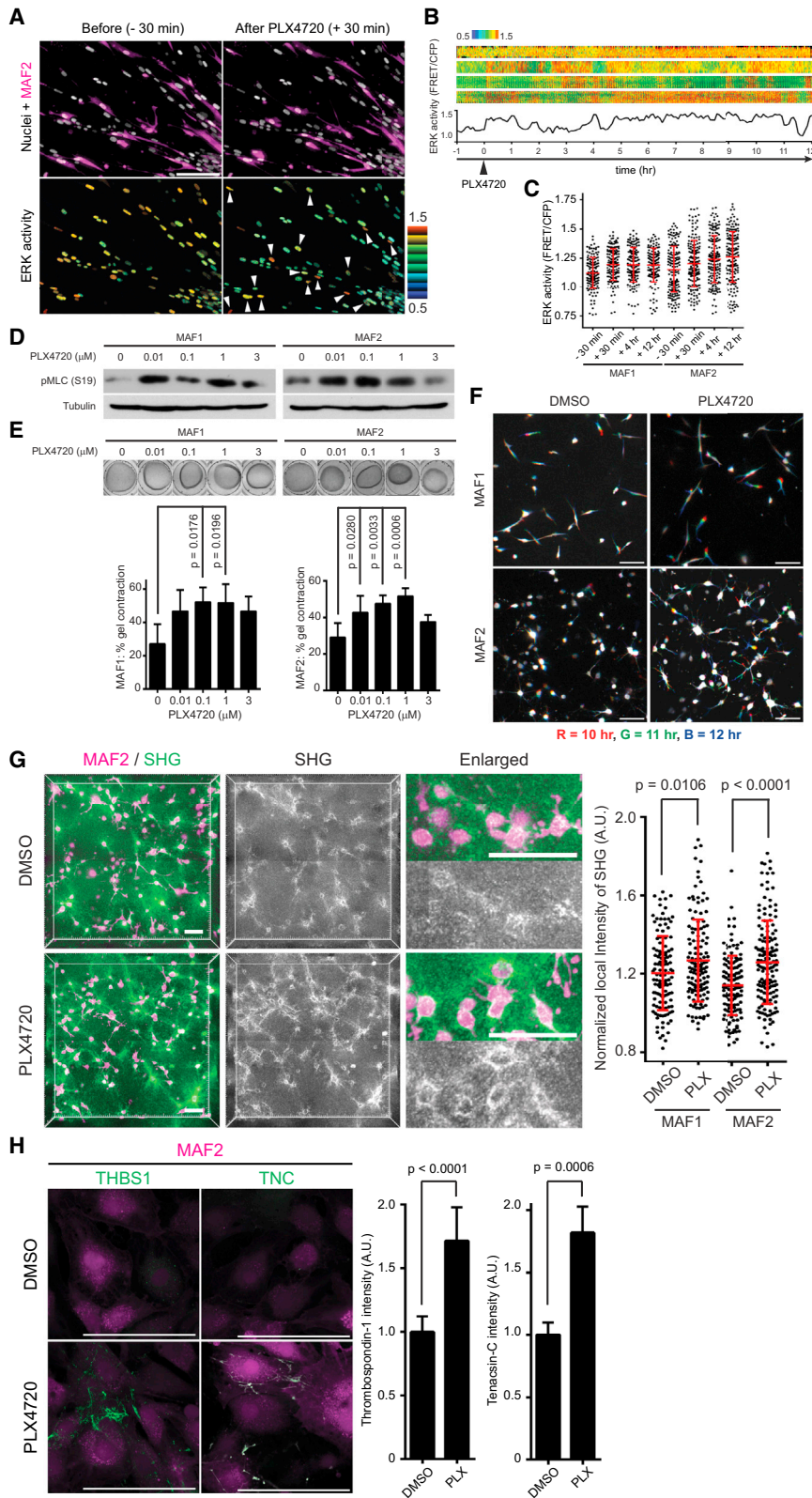
Figure 3. PLX4720 Paradoxically Activates Melanoma-Associated Fibroblasts

(A–C) 5555-EKAREV-NLS and MAF1/2-EKAREV-NLS-mCherry co-cultured spheroids were embedded in collagen gels and treated with PLX4720 (1 μM) at time = 0. Upper images in (A) indicate 5555 and MAF2 nuclei (gray) and MAF2 (magenta), and lower images indicate ERK activity (FRET/CFP) in 5555 and MAF2 (pointed by arrowheads) before (−30 min) and after (+30 min) treatment. Kymographs of ERK activity in five representative MAF2 cells are shown in (B), and ERK activities at time −30 min, +30 min, +4 hr, and +12 hr are quantified and shown in (C) as scatterplots with mean ± SD. Scale bar represents 100 μm.

(D) Immunoblotting for indicated proteins in MAF1/2 treated with different concentrations of PLX4720 (0–3 μM).

(E) Representative images and quantification of gel contraction by MAF1/2 treated with different concentrations of PLX4720 (0–3 μM). Histograms show quantification of three independent experiments (mean ± SD).

(F) Motion analysis of MAF1/2 in the gel contraction assay treated with 0.1% DMSO or PLX4720 (1 μM), in which three different time points are shown overlain in red (10 hr), green (11 hr), and blue (12 hr). Scale bars represent 100 μm.

(G) Representative images of MAF2 and second harmonic generation (SHG) in the gel contraction assay. Local SHG intensities around MAFs were calculated and quantified by normalizing to the background signals. Each dot indicates SHG signal from a single MAF, and bars indicate mean ± SD. Scale bars represent 100 μm.

(H) Immunostaining of non-permeabilized MAF2 (in magenta) with anit-thrombospondin-1 (THBS1) and anti-tenascin-C (TNC) antibodies, treated with DMSO (0.1%) or PLX4720 (1 μM) for 24 hr. Relative fluorescence intensity of THBS1 and TNC are quantified and shown (mean ± SD).

Scale bars represent 100 μm. See also Figure S3 and Movies S2 and S3.

two kinase inhibitors that target PDGFR in common. These experiments demonstrate that PLX4720 enhances RTK-dependent functions of MAFs.

ECM Composition and Stiffness Cooperate to Provide Tolerance to PLX4720

The data above show that PLX4720 elicits changes in matrix production and remodeling by MAFs. To test if the ECM was sufficient to modulate the response of melanoma cells to PLX4720, we varied both matrix composition and matrix stiffness. Figure S4A shows that fibronectin (FN) consistently reduces the effect of PLX4720 on both 5555 and 4434 melanoma cells. Other matrix components, including THBS1/2 and TNC, have more variable effects between the two cell lines. In addition to matrix

PDGFR on both basal and PLX-induced matrix remodeling by MAFs. Figure S3G shows that both basal and PLX4720-induced MAF activity were greatly reduced by imatinib and sunitinib,
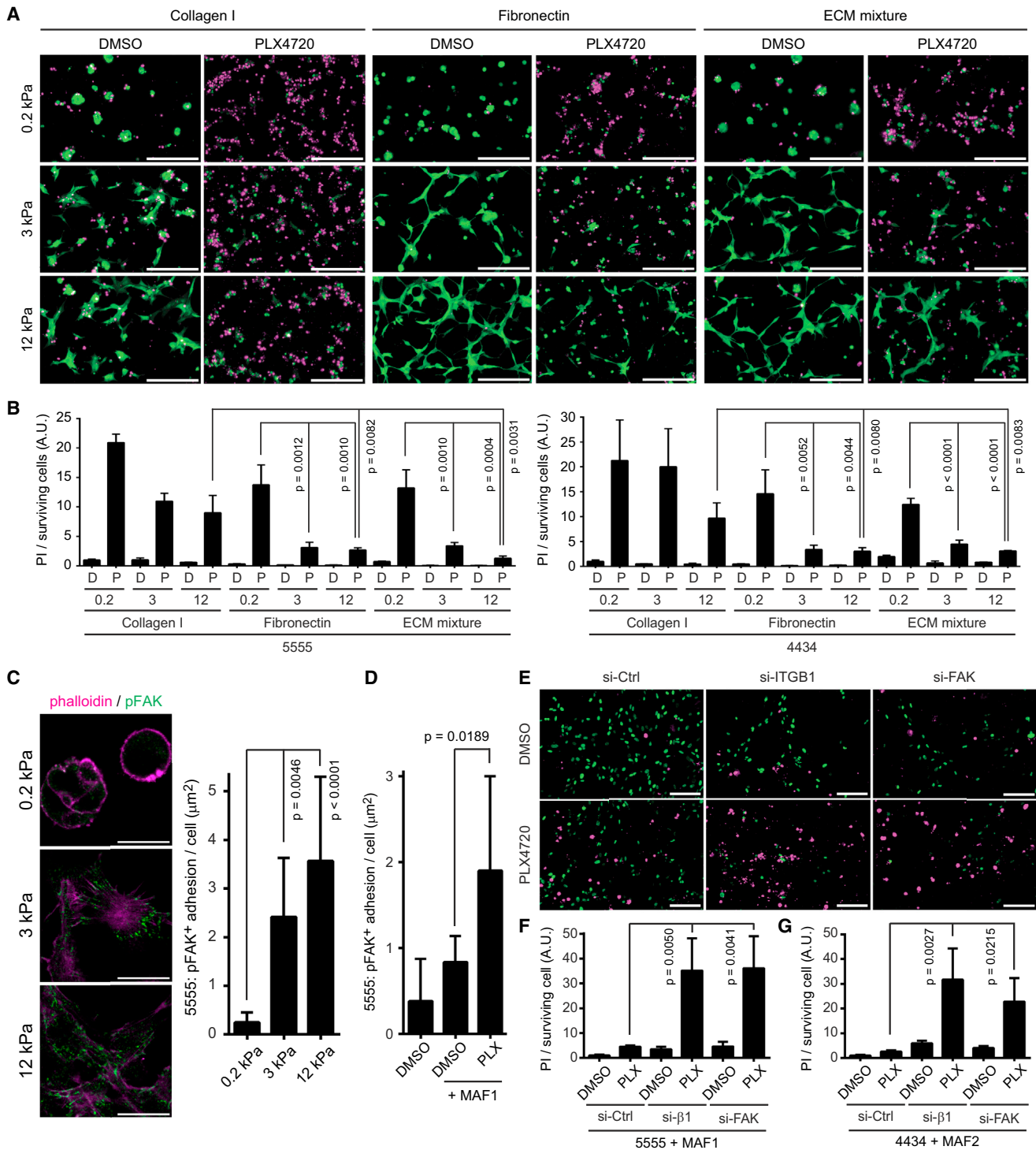
Figure 4. ECMs and Rigid Substrates Mediate Drug Tolerance through Integrin β1-FAK Activation

(A and B) 5555-mEGFP (in green) were seeded on polyacrylamide / bis-acrylamide gels with different stiffness (0.2, 3 and 12 kPa) coated with the indicated ECMs (ECM mixture contains FN, TNC, THBS1, and THBS2). Twenty-four hours after treatment with DMSO (0.1%) or PLX4720 (1 μM), cells are stained with propidium iodide (PI, in magenta). PI signals from the same experiments with 5555/4434-YFP-NLS were quantified in (B) (mean ± SD). Scale bars represent 100 μm.

(C) 5555 cells cultured on the fibronectin-coated gels with the indicated stiffness were stained with a phospho-FAK antibody. The area of pFAK positive adhesion is quantified (mean ± SD). Scale bars represent 100 μm.

(D) 5555 cells co-cultured with or without MAF1 on collagen gels were treated with DMSO (0.1%) or PLX4720 (1 μM) for 24 hr and stained with a phospho-FAK antibody. The area of pFAK positive adhesion in 5555 cell is quantified and shown as mean ± SD.

(legend continued on next page)

composition, matrix stiffness affects the behavior of cancer cells. Therefore, we combined variations in matrix composition and matrix stiffness. Polyacrylamide gels ranging from 0.2 kPa (similar to adipose tissue) to 12 kPa (similar to stiff tumors or muscle) were coated with either collagen I, FN, or a combination of FN, THBS1/2, and TNC. Melanoma cells on low stiffness collagen I showed high levels of cell death following BRAF inhibition (Figures 4A and 4B). However, this was greatly abrogated if cells were cultured on FN matrices with either 3 kPa or 12 kPa stiffness, with the most impressive cell survival on 12 kPa FN-, THBS1/2-, and TNC,containing matrices (Figures 4A and 4B). These data demonstrate that an appropriate matrix composition and stiffness can render BRAF-mutant melanoma cells insensitive to PLX4720.

Integrin β1 and FAK Signaling Leads to ERK Re-activation in Melanoma Cells

Increasing the stiffness of fibronectin matrices lead to the re-organization of integrin β1 into focal adhesions and elevated pFAK levels (Figures 4C and S4B). Furthermore, treatment of co-cultures with PLX4720 led to the relocation of active integrin β1 into fibrillar adhesions and increased pFAK signals (Figures 4D and S4C). To determine if the changes in integrin organization and FAK signaling are relevant for the adaptation of melanoma-MAF co-cultures to PLX4720, we investigated the effect of combined PLX4720 treatment and experimental perturbation of integrin β1 and FAK. Combination of PLX4720 with either integrin β1 or FAK depletion led to prevention of ERK/MAPK re-activation and synergistic induction of cell death (Figures 4E–4G, S4D, and S4E).

We next investigated whether combining BRAF inhibition with pharmacological targeting of signaling downstream of integrin β1 would be effective. Multiple FAK inhibitors (PF573228, PF562271, FAKi14) prevented the re-activation of ERK/MAPK signaling in melanoma/MAF co-cultured spheroids treated with PLX4720 (Figures 5A, 5C, S5A, and S5B and Movie S4, see also Figure 2E; all quantification is collated in Figure S5G, and similar results with 4434 cells in Figures S5H and S5I). Treatment of PLX4720-naive cells with FAK inhibitors alone did not lead to reduced ERK activity (Figures 5A, 5C, S5A, and S5B). As expected, combined BRAF and MEK inhibition lead to a stable reduction in ERK activity (Figures 5C and S5C).

In accordance with the results of EKAREV FRET imaging, combination of PLX4720 with FAK inhibition led to synergistic induction of cell death in the co-cultured spheroids (Figure 5D). These combinations were equally as effective as PLX4720 combined with PD184352. Because FAK activity is often linked to Src function, we tested the effect of two Src inhibitors in combination with PLX4720. Both dasatinib and PP2 effectively prevented the re-activation of ERK signaling following PLX4720 treatment (Figures 5B, 5C, and S5D and Movie S4). Furthermore, the combination of PLX4720 and dasatinib led to significantly increased melanoma cell death (Figure 5D). Neither FAK nor

Src inhibition reduced the viability of melanoma mono-cultures (Figure S5J). These data demonstrate the critical role of adhesion-mediated signaling via integrin β1, FAK, and Src in the adaptive re-activation of ERK/MAPK following BRAF inhibition in tumor/stroma co-cultures.

Both basal and PLX4720-enhanced MAF activity can be reduced by targeting PDGFR (Figure S3G). This predicts that PDGFR inhibition should also synergize with PLX4720 to reduce ERK activity. We tested this by monitor EKAREV signals following the combination of PLX4720 and imatinib (autofluorescence of sunitinib prevented us from testing its effect in this assay). This combination reduced the re-activation of ERK, while imatinib alone had no effect (Figures S5E and S5F). These data support our hypothesis that PDGFR signaling in the stroma contributes to ERK re-activation in melanoma cells.

We next tested whether BRAF and FAK inhibition would synergize to control melanoma growth in vivo. 5555 melanoma tumors were allowed to reach 4–8 mm before mice began receiving daily doses of PLX4720, PF562271, PLX4720 and PF562271, or vehicle. Figure 5E shows that only the combination of BRAF and FAK inhibitors led to effective control of tumor size; either inhibitor alone had only a modest effect. PLX4720-treated tumors had increased aligned fibrous ECM and FN, and this was associated with FAK-dependent elongation of melanoma cells (Figure 5F). These data indicate that combined BRAF and FAK inhibition is a promising strategy for improving management of BRAF mutant melanoma.

Stromal Support for Residual Disease in Models Exhibiting Incomplete Responses to PLX4720

The data described above demonstrate that MAFs provide a mechanism for mouse BRAF-mutant melanoma cell lines refractory to PLX4720 in vivo. However, the majority of human BRAF-mutant melanoma respond well to BRAF inhibition before the emergence of resistant disease over many months (Chapman et al., 2011). We were interested whether our findings regarding the role of the stroma in providing drug tolerance were relevant to the survival of melanoma cells in between the initial administration of BRAF inhibitors and the ultimate emergence of genetically resistant cells. Therefore, we examined ERK/MAPK activity and stromal changes in two models of human melanoma that exhibit a clear response to BRAF inhibition in vivo. Figures 6A and 6B show that A375 and WM266.4 human melanoma cells are sensitive to PLX4720 both in vitro and in vivo. However, tumors did not disappear and typically 2–4 mm of residual disease remained during PLX4720 treatment. We hypothesized that this residual disease may be supported by signals from the stroma. Intravital imaging of the EKAREV biosensor revealed that the residual disease after 11–14 days of PLX4720 treatment exhibited similar levels of ERK/MAPK signaling to the pre-treatment tumors (Figures 6C and S6A). Based on our analysis of 5555 and 4434 models, we predict the following: there should be changes in the stroma of PLX4720-treated A375 and WM266.4 tumors,

(E) 5555-YFP-NLS (in green) transfected with the indicated siRNAs were co-cultured with MAF1 overnight. Then, cells were treated with DMSO (0.1%) or PLX4720 (1 μM) for 24 hr, followed by PI staining (in magenta). Scale bars represent 100 μm.
(F) PI signals of (E) were quantified and shown as mean ± SD (G) PI signals from same experiments as in (E) using 4434 + MAF2 co-cultures were quantified and shown as mean ± SD.
See also Figure S4.
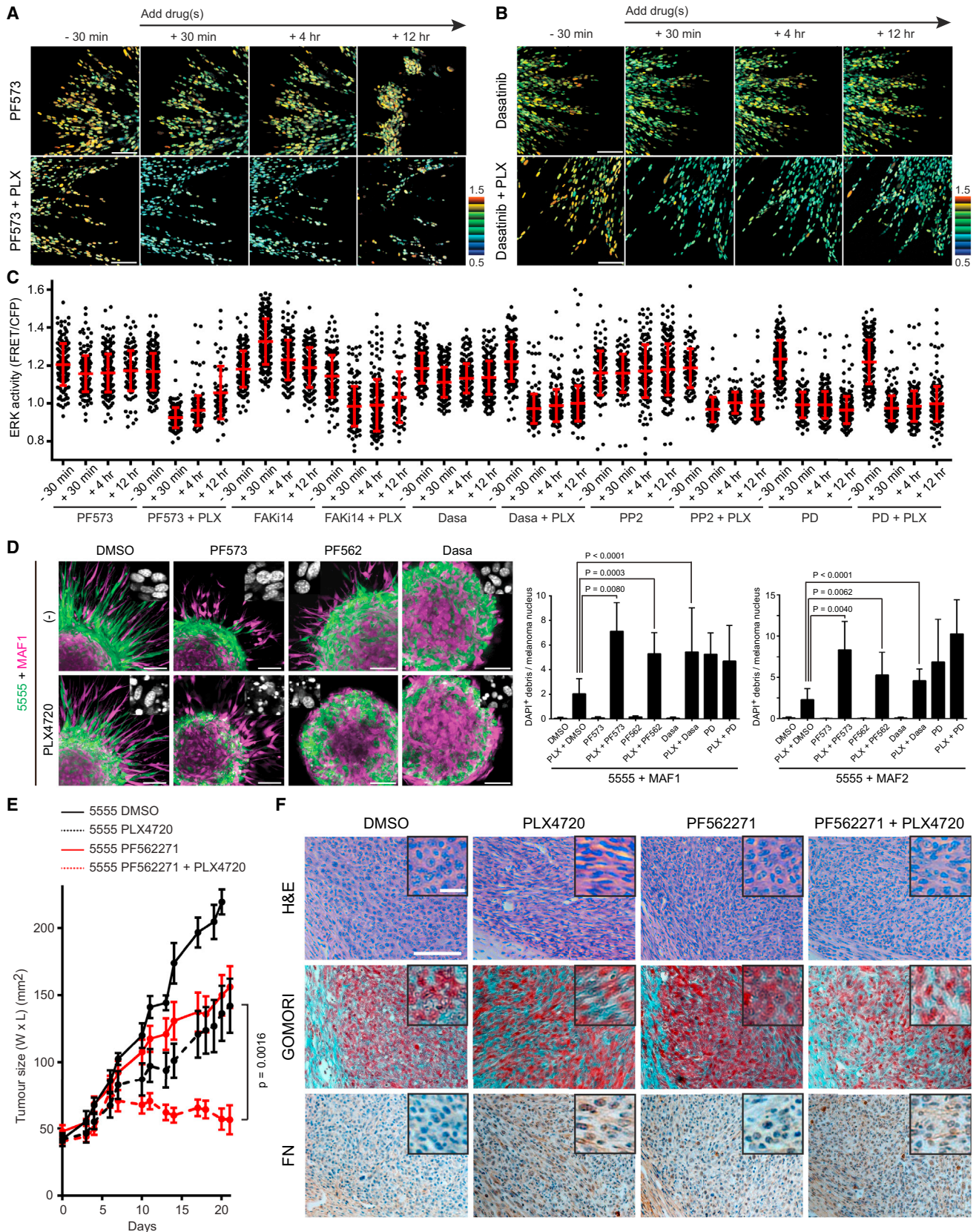
(legend on next page)

the melanoma cells should not be intrinsically resistant to PLX4720 at this stage, but that they should use FAK- and Src-dependent signaling to sustain ERK/MAPK activity and survival. Both A375 and WM266.4 exhibited clear changes in collagen SHG when treated with PLX4720 (Figure 6C). This is consistent with increased matrix deposition and remodeling by fibroblasts. Immunohistochemical staining, and Gomori's trichrome staining confirmed that the residual disease was rich in fibroblastic stroma and had higher levels of fibrillar collagen, FN and TNC (Figures 6D and S6A). Furthermore, conformation specific antibodies revealed increased active integrin β1 levels in PLX-treated tumors (Figure S6B).

To formally confirm that the melanoma cells were dependent on extrinsic signals for their tolerance of PLX4720, we re-isolated A375 and WM266.4 cells from the residual disease that persisted following PLX4720 treatment. Figure S6C shows that these cells are just as sensitive to PLX4720 as parental cells when cultured in isolation without a supportive tumor microenvironment. These data demonstrate the persistence of residual disease is due to cell extrinsic factors that re-activate ERK signaling by a BRAF-independent mechanism. To further test our hypothesis, we investigated whether the ERK signaling in residual disease was dependent on FAK and Src function. Combination of either PF573228 or dasatinib with PLX4720 led to more prolonged ERK inhibition in tumor explants (Figure S6D). Finally, we tested whether combining BRAF and FAK inhibition would have a synergistic effect on A375 tumor burden. Established A375 tumors (5–7 mm) were treated with PLX4720, PF562271, PLX4720, and PF562271, or vehicle for up to 30 days. We observed that combined BRAF and FAK inhibition led to significantly reduced burden compared to either treatment alone (Figure 6E); indeed, no bioluminescence signal could be detected in one mouse. Co-targeting BRAF and FAK also triggered extensive neutrophil and macrophage infiltration (Figure S6E). More surprisingly, although PLX4720 controls total melanoma volume in this tumor model, it has a minimal effect on Ki-67 positivity, whereas PLX4720 + PF562271 leads to a clear reduction in Ki-67 positive melanoma cells (Figures 6F and 6G). These data suggest that PLX4720-treated tumors continue to proliferate, albeit balanced by cell death. This would enable the evolution of resistant clones even in a PLX4720-treated tumor that is not increasing in size.

We next investigated changes in the tumor stroma and the effect of FAK inhibition in a patient-derived xenograft (PDX) model. A PDX was established from a vemurafenib naive BRAF mutant melanoma. Figure 7A shows that this grows well in control NOD.Cg-Prkdc[scid] Il2rg[tm1Wjl]/SzJ (NSG) mice, but the growth of this PDX was controlled by PLX4720, although sig-

nificant disease remained. In agreement with our analyses of A375 and WM266.4 tumors, histological analysis of the residual disease in PLX4720-treated mice revealed increased fibrous ECM, higher numbers of αSMA-positive cells, and active ERK/MAPK signaling (Figure 7B). We next explored whether this PDX model would eventually fail PLX4720 therapy, and whether FAK inhibition might reduce this failure. After roughly 50 days of PLX4720 treatment, the PDX tumors began to grow, indicating therapy failure (Figure 7C). FAK inhibition alone had no effect on tumor growth, but when combined with PLX4720 lead to significantly increased tumor control both at early time points and, more importantly, after 4 months when PLX4720-treated tumors were failing therapy (Figure 7C). No adverse effects, such as weight loss, were observed in mice treated with PLX4720 and PF562271 for 4 months (Figure S7A).

Alterations in Tumor Stroma and ECM in Vemurafenib-Treated Patients

The data above demonstrate that BRAF inhibition can directly affect the fibroblastic stroma leading to remodeled ECM and adhesion-dependent signaling to ERK that negates the effect of BRAF inhibition in the melanoma cells. We find histologic features that are compatible with our experimental models in patient samples prior to vemurafenib treatment and following disease progression on vemurafenib (Table S2): these include changes in the stroma and melanoma cell morphology following vemurafenib treatment. Figure S7B shows increased fibrous ECM and αSMA-positive MAFs were visible in Patients 1 and 4 after failure of BRAF inhibition. In Patient 4, there was an increase in elongated melanoma cells. These analyses confirm that BRAF inhibition can modulate the fibrous ECM and fibroblastic stroma in melanoma patients. Taken together with the experimental work, we show how an effect of BRAF inhibition on the stroma generates a drug-tolerant microenvironment that supports residual disease before the emergence of genetic cell intrinsic drug resistance mechanisms (Figure 7D).

DISCUSSION

A common feature of kinase-targeted therapies is a period of response followed by the emergence of resistant disease. In melanoma, different genetic resistance mechanisms can develop in the same patient (Shi et al., 2014; Van Allen et al., 2014), often at multiple metastatic sites (Shi et al., 2014). These data are not easily reconciled with a model of a pre-existing genetically resistant sub-clone; thus, resistant melanoma cells may arise after treatment with vemurafenib has begun.


Figure 5. Simultaneous Inhibition of BRAF and FAK Effectively Induces Cell Death in 5555 Cells

(A–C) 5555-EKAREV-NLS and MAF1-mCherry co-cultured spheroids were embedded in collagen gels and treated with indicated drugs: PF573228 (1 μM), FAK inhibitor 14 (1 μM), dasatinib (200 nM), PP2 (1 μM) ± PLX4720 (1 μM). ERK activities at time −30 min, +30 min, +4 hr, and +12 hr are quantified and shown in (C) as scatterplots with mean ± SD. Scale bars represent 100 μm.

(D) 5555-mEGFP (green) and MAF1/2-mCherry (magenta) co-cultured spheroids were embedded into collagen gels and treated with 0.1% DMSO, PF573228 (1 μM), PF562271 (1 μM), dasatinib (200 nM) ± PLX4720 (1 μM) for 48 hr. Representative DAPI-staining images are also shown in each image, and the ratio of DAPI-positive debris and melanoma nucleus was calculated and shown as mean ± SD. Scale bars represent 100 μm.

(E and F) 5555 cells were subcutaneously allografted in C57BL/6 mice and treated with DMSO (4%), PLX4720 (25 mg/kg), PF562271 (50 mg/kg), or the combination. Tumor growth in each group is shown in (E) (mean ± SD, nine mice in control group and ten mice in other groups), and representative images of H&E, Gomori trichrome (collagen fibers in bright blue), and anti-fibronectin staining are shown in (F).

Enlarged view is also shown as an inset on each image. Scale bars represent 100 μm (low magnification) and 20 μm (high magnification). See also Figure S5 and Movie S4.
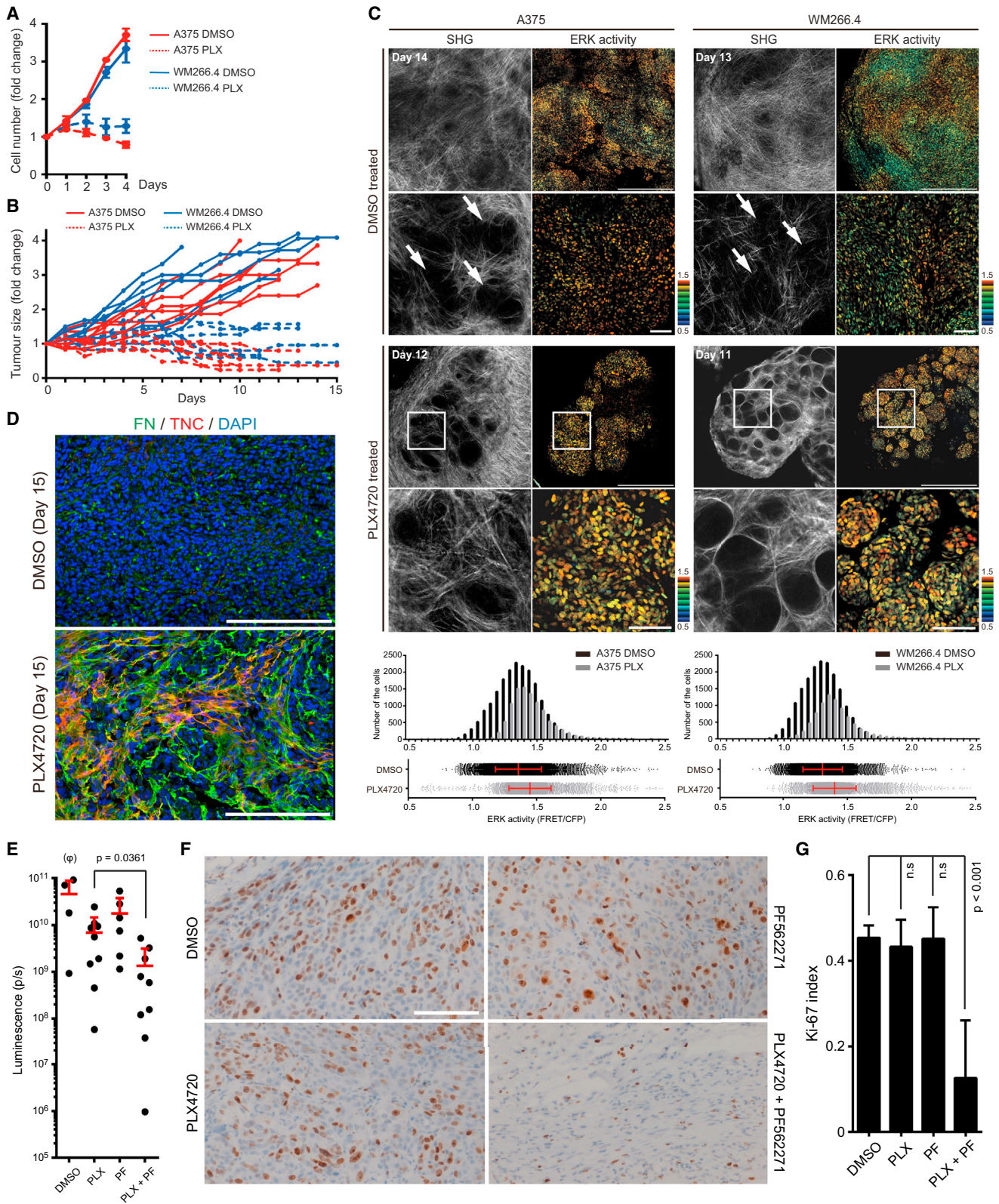
Figure 6. Stromal Cells Provide Safe Haven to Tolerate BRAF Inhibition for Drug-Sensitive Human Melanoma Cells

(A and B) Growth curves of the indicated melanoma cells in vitro (A) (mean ± SD) and in vivo (B) treated with DMSO (0.1% in vitro and 4% in vivo) or PLX4720 (1 μM in vitro and 25 mg/kg in vivo).

(legend continued on next page)

How significant numbers of BRAF-mutant cells survive therapy prior to the emergence of genetic mutations or epigenetic changes that enable resistance is not well understood, and here we describe a mechanism enabling the survival of large numbers of BRAF-mutant melanoma cells following PLX4720 treatment. This mechanism has two key features: first, the fibroblastic stroma is "paradoxically" activated by BRAF inhibition; and second, adhesion-dependent signals from the altered tumor microenvironment lead to BRAF-independent ERK/MAP kinase activity.

BRAF inhibitors can promote Ras-driven signaling through CRAF (Hatzivassiliou et al., 2010; Heidorn et al., 2010; Nazarian et al., 2010; Poulikakos et al., 2010; Villanueva et al., 2010); however, it was not clear if this mechanism may act on Ras-signaling in the stroma and how this may affect therapeutic efficacy. We find that PLX4720 increases ERK/MAPK signaling, elevates matrix production, and increases MLC phosphorylation and matrix remodeling, which is likely due to enhancing RTK-Ras signaling. These compounds probably act through their effects on PDGFR, which is upregulated by PLX4720 and has previously been implicated in the function of carcinoma-associated fibroblasts (Erez et al., 2010; Kalluri and Zeisberg, 2006; Pietras et al., 2008). Dabrafenib is likely to activate the fibroblastic stroma in a similar manner to PLX4720 (Gibney and Zager, 2013; Huang et al., 2013). Interestingly, we found that PLX4720 did not enhance the activity of normal fibroblasts; this may be because they do not have elevated RTK signaling.

The ability of MAFs to confer PLX4720 tolerance depends on integrin β1 and FAK in the melanoma cells. Furthermore, fibronectin-rich matrices of the appropriate stiffness are sufficient to abrogate the effects of BRAF inhibition. We propose that certain ECM environments provide "safe havens" for melanoma cells to tolerate BRAF targeted therapy. Although extrinsic signals from the tumor microenvironment can support four different BRAF-mutant melanoma cell lines in the presence of PLX4720, the magnitude of this protective effect varied—these models recruit stroma with different composition and different degrees of activation. Therefore, the magnitude of the effect of PLX4720 on the stroma would be variable. Alternatively, melanoma cells may differ in their ability to activate adhesion-dependent FAK and Src to ERK/MAP kinase. Although we find no role for HGF in our analyses, the ability of c-Met to drive Rac activation and elongated modes of cell migration could be a point of commonality with the work of Strausmann et al. (Straussman et al., 2012;

Watson et al., 2014). Furthermore, the relief of negative inhibition that can be triggered by BRAF inhibition may also sensitize melanoma cells to integrin/FAK-mediated ERK activation (Lito et al., 2012, 2013).

There are currently moves to use combined blockade of BRAF and MEK to improve outcomes in melanoma (Flaherty et al., 2012; Wagle et al., 2014). Although this approach extends lifespan, it is rarely curative (Larkin et al., 2014). We find that BRAF and FAK inhibition is another promising strategy. Both strategies are similarly effective at inducing melanoma cell death. In the long term, combined BRAF and FAK blockade improves tumor control but rarely eliminates tumors entirely, and some PDX tumors resume very slow growth after 2–3 months. The lack of cure may reflect problems in drug access. Our results also indicate that BRAF and Src inhibition will be effective and recent results using a combined RAF and SRC inhibitor support this (Girotti et al., 2015). Furthermore, because many RTKs require signals from cell adhesions to function (Butcher et al., 2009; Paszek et al., 2005; Sulzmaier et al., 2014), FAK targeting may attenuate divergent signaling from cell adhesion receptors and RTKs to cell survival and proliferation machinery, and this may provide some benefit over simply targeting ERK signaling.

To conclude, multiple mechanisms of cell-intrinsic resistance to melanoma have been documented. In patients, cell-intrinsic resistance to vemurafenib typically emerges over a period of months. The mechanisms that sustain melanoma cells in the period between initial response and disease progression on therapy are unclear. We describe how paradoxical activation of the fibroblastic stroma enables matrix-derived signaling via integrin β1 and FAK to promote ERK activation and cell survival. This could sustain the pool of melanoma cells from which intrinsic resistant clones emerge. We propose that by reducing the numbers of residual melanoma cells, there would less material from which truly resistant cells could arise. This should lead to longer periods of progression-free survival and possibly even cure.

EXPERIMENTAL PROCEDURES

Cells and Probes

BRAF-mutant (5555 and 4434) and NRAS-mutant (C790) mouse melanoma cell lines were established from C57BL/6_BRAF +/LSL-BRAFV600E ; Tyr::CreERT2/o (Dhomen et al., 2009) and C57BL/6_NRAS +/LSL-NRASG12D ; Tyr::Cre-A (Pedersen et al., 2013), respectively. B16F10 mouse melanoma cell lines, and A375 and WM266.4 human melanoma cell lines were a gift from Prof. Chris Marshall (Institute of Cancer Research, London, UK).

(C) Intravital images of A375- and WM266.4-expressing EKAREV-NLS in nude mice. Images are from mice treated with DMSO (4%) or PLX4720 (25 mg/kg) for the indicated days. Arrows in high magnification images of DMSO-treated tumors indicate small cages created by thick collagen fibers (detected by second harmonic generation: SHG). In PLX4720-treated tumors, the regions in white squares are magnified and shown below. Distribution (scatterplots with mean ± SD) and histogram of ERK activities in A375 and WM266.4 tumors are shown at the bottom. Scale bars represent 500 μm (low magnification) and 100 μm (high magnification).

(D) Frozen sections of WM266.4 tumors treated with DMSO or PLX4720 for 15 days were double-stained with anti-fibronectin (in green) and anti-tenascin-C (in red) antibodies. Scale bars represent 200 μm.

(E) A375 cells stably expressing firefly luciferase grown subcutaneously in nude mice were treated with DMSO (4%), PLX4720 (25 mg/kg), PF562271 (50 mg/kg), or the combination. Bioluminescence from the tumors was analyzed at day 25 and shown (mean ± SD). (φ) Please note that DMSO group (n = 4) contains fewer mice than other groups because the higher growth rates of these tumors meant that some mice were killed before day 25.

(F) A375 tumors treated with the indicated drug(s) for 29 days were stained with an anti-Ki-67 antibody. Scale bar represents 100 μm.

(G) Ki-67 index was measured from three different positions in six different tumors treated with the indicated drugs for 18–29 days.

Data are represented as mean ± SD. Please note that necrotic areas with myeloid cell infiltration in PLX4720 + PF562271 tumors were excluded from the analysis. See also Figure S6.
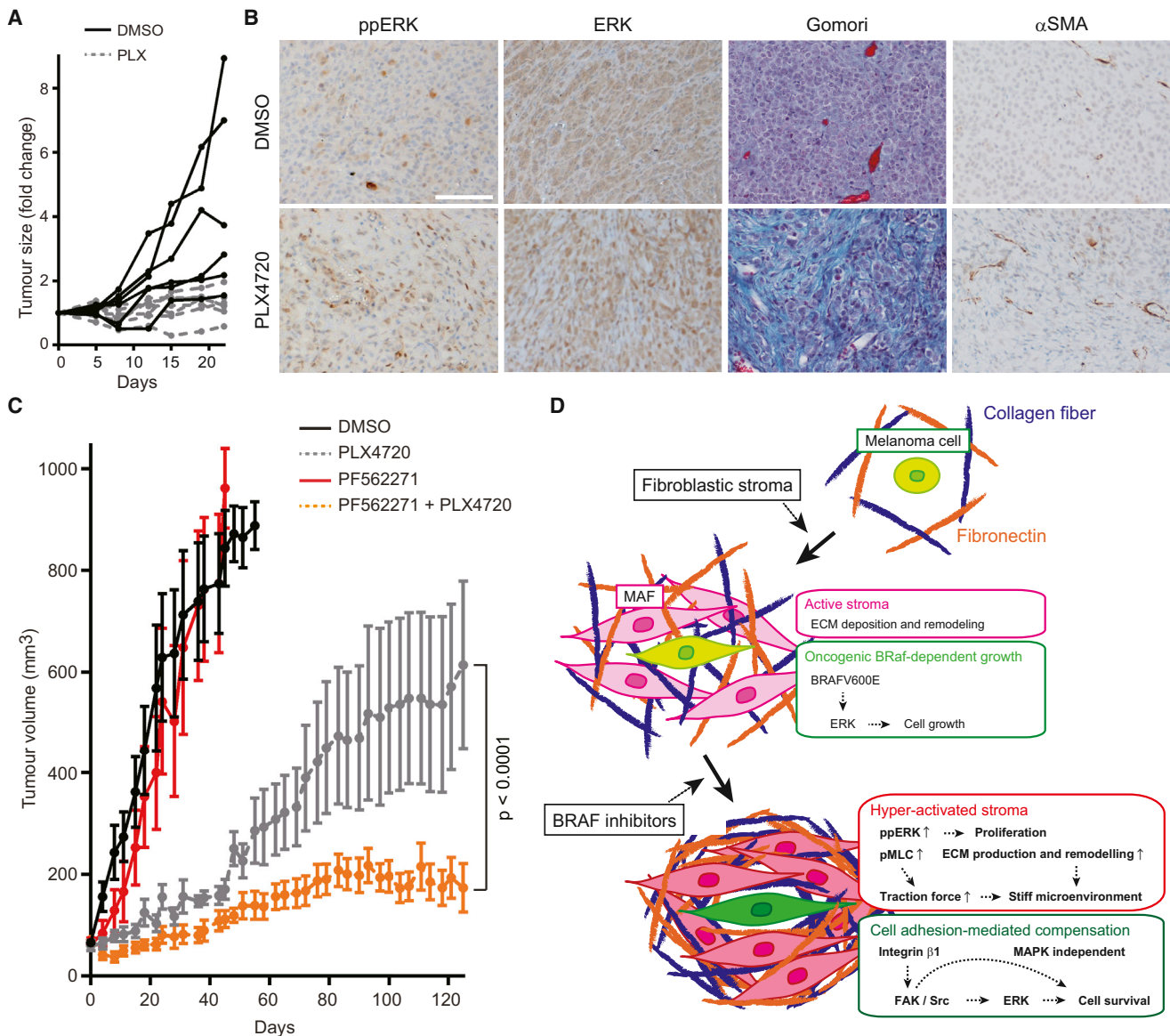
Figure 7. Combinatorial Inhibition of BRAF and FAK Suppresses the Growth of Patient-Derived Xenograft

(A) Growth curves of vemurafenib-naive patient derived xenograft (PDX) in IL-2 NSG mice treated with DMSO (5%) or PLX4720 (45 mg/kg) for 22 days.

(B) Anti-phospho-ERK, anti-ERK, Gomori trichrome, and anti-αSMA staining of the fixed PDX samples treated with DMSO or PLX4720 for 22 days. Scale bars represent 100 μm.

(C) Growth curves of PDX treated with DMSO (4%), PLX4720 (45 mg/kg), PF562271 (50 mg/kg), or the combination. Data are represented as mean ± SD, seven mice per group.

(D) Scheme of drug tolerance mechanisms against BRAF selective inhibitors.

See also Figure S7.

Melanoma cells were maintained in DMEM (Invitrogen) with 10% fetal bovine serum/1% PenStrep (GIBCO). The FRET biosensors for ERK/MAPK (EKAREV-NLS/NES) was described previously (Komatsu et al., 2011) and were introduced into the cells with *PiggyBac* transposon system (Wellcome Trust Sanger Institute, Hinxton, UK).

Mouse Allograft/Xenograft Model

Animal experiments were done in accordance with UK regulations under project license PPL/80/2368. For melanoma allograft model, 2×10^6 5555 or 4434 cells were suspended into 200 μl PBS and subcutaneously injected in the flanks of C57BL/6 mice or C57BL/6_ROSA26_mTmG mice. After

10–14 days when the cells form palpable tumors, the mice were dosed daily by oral gavage with vehicle (4% DMSO), PLX4720 (25 mg/kg), PF562271 (50 mg/kg), or the combination. The tumor size was monitored daily by calculating length × width (mm²). For experimental lung metastasis, 2×10^6 5555 cells in 200 μl PBS were injected from the tail vein and, after 4 weeks, the mice were killed and the lung tumors are examined further. For human melanoma xenograft model, 2×10^6 A375 or WM266.4 cells in 200 μl PBS were subcutaneously injected in the flanks of nude mice. After about 2 weeks when palpable tumors formed, we started further experiments. For skin-flap tumor imaging, the mouse was anesthetized and the tumor was surgically exposed and imaged through a coverslip with a Zeiss LSM780 inverted

microscope as described elsewhere (Giampieri et al., 2009). For bioluminescence imaging, nude mice bearing A375 tumors stably expressing firefly luciferase were anesthetized, intraperitoneally injected with D-Luciferin (150 mg/kg, PerkinElmer), and imaged under IVIS Spectrum (PerkinElmer).

Patient Samples and Patient-Derived Xenografts

Tumor samples were collected under the Manchester Cancer Research Centre (MCRC) Biobank ethics application no. 07/H1003/161+5 with full informed consent from the patients. The work presented in this manuscript was approved by MCRC Biobank Access Committee application 13_RIMA_01. Metastatic melanoma tumor samples from vemurafenib-resistant patients (nos. 1–5) and from a vemurafenib-naive patient (no. 6) were obtained immediately after surgery. For PDX models, necrotic parts of the tumors were removed and $5 \times 5 \times 5$ mm pieces were implanted subcutaneously in the right flanks of 5- to 6-week-old female IL-2 NSG mice. When the PDXs reached 1500 mm^3 volume, they were excised, and viable tissue was dissected into 5 mm cubes and transplanted into additional mice using the same procedure. Genomic and histological analyses had confirmed that the tumors at each point were derived from the starting material. Following transplantation, tumors were allowed to grow to ~60–80 mm^3, and the mice were randomized before initiation of treatment by daily orogastric gavage of PLX4720 (45 mg/kg), PF562271 (50 mg/kg), vehicle (5% DMSO, 95% water), or the combination for the indicated days.

Time-Lapse FRET Imaging of Cultured Melanoma Spheroids

Tumor spheroids cultured in collagen gel on a glass bottom dish/plate were imaged with an LSM780 inverted microscope through 20× objective every 5 min for up to 13 hr. For the dual-emission ratio imaging, the FRET biosensor was excited by a Chameleon Ti:sapphire Laser (Coherent Inc.) at 820 nm excitation wavelength. The emission light was separated by beam splitters into 463–506 nm for CFP and 515–559 nm for FRET. Details in microscopy, data analysis, and image processing are available in the Supplemental Experimental Procedures.

ACCESSION NUMBERS

The National Center for Biotechnology Information's Gene Expression Omnibus database accession number for the microarray data sets is GSE63160.

SUPPLEMENTAL INFORMATION

Supplemental information includes Supplemental Experimental Procedures, seven figures, two tables, and four movies and can be found with this article online at http://dx.doi.org/10.1016/j.ccell.2015.03.008.

REFERENCES

Butcher, D.T., Alliston, T., and Weaver, V.M. (2009). A tense situation: forcing tumour progression. Nat. Rev. Cancer 9, 108–122.

Calvo, F., Ege, N., Grande-Garcia, A., Hooper, S., Jenkins, R.P., Chaudhry, S.I., Harrington, K., Williamson, P., Moeendarbary, E., Charras, G., and Sahai, E. (2013). Mechanotransduction and YAP-dependent matrix remodelling is required for the generation and maintenance of cancer-associated fibroblasts. Nat. Cell Biol. 15, 637–646.

Chapman, P.B., Hauschild, A., Robert, C., Haanen, J.B., Ascierto, P., Larkin, J., Dummer, R., Garbe, C., Testori, A., Maio, M., et al.; BRIM-3 Study Group (2011). Improved survival with vemurafenib in melanoma with BRAF V600E mutation. N. Engl. J. Med. 364, 2507–2516.

Dhomen, N., Reis-Filho, J.S., da Rocha Dias, S., Hayward, R., Savage, K., Delmas, V., Larue, L., Pritchard, C., and Marais, R. (2009). Oncogenic Braf induces melanocyte senescence and melanoma in mice. Cancer Cell 15, 294–303.

Druker, B.J., Talpaz, M., Resta, D.J., Peng, B., Buchdunger, E., Ford, J.M., Lydon, N.B., Kantarjian, H., Capdeville, R., Ohno-Jones, S., and Sawyers, C.L. (2001). Efficacy and safety of a specific inhibitor of the BCR-ABL tyrosine kinase in chronic myeloid leukemia. N. Engl. J. Med. 344, 1031–1037.

Druker, B.J., Guilhot, F., O'Brien, S.G., Gathmann, I., Kantarjian, H., Gattermann, N., Deininger, M.W., Silver, R.T., Goldman, J.M., Stone, R.M., et al.; IRIS Investigators (2006). Five-year follow-up of patients receiving imatinib for chronic myeloid leukemia. N. Engl. J. Med. 355, 2408–2417.

Erez, N., Truitt, M., Olson, P., Arron, S.T., and Hanahan, D. (2010). Cancer-associated fibroblasts are activated in incipient neoplasia to orchestrate tumor-promoting inflammation in an NF-kappaB-dependent manner. Cancer Cell 17, 135–147.

Flaherty, K.T., Puzanov, I., Kim, K.B., Ribas, A., McArthur, G.A., Sosman, J.A., O'Dwyer, P.J., Lee, R.J., Grippo, J.F., Nolop, K., and Chapman, P.B. (2010). Inhibition of mutated, activated BRAF in metastatic melanoma. N. Engl. J. Med. 363, 809–819.

Flaherty, K.T., Infante, J.R., Daud, A., Gonzalez, R., Kefford, R.F., Sosman, J., Hamid, O., Schuchter, L., Cebon, J., Ibrahim, N., et al. (2012). Combined BRAF and MEK inhibition in melanoma with BRAF V600 mutations. N. Engl. J. Med 367, 1694–1703.

Giampieri, S., Manning, C., Hooper, S., Jones, L., Hill, C.S., and Sahai, E. (2009). Localized and reversible TGFbeta signalling switches breast cancer cells from cohesive to single cell motility. Nat. Cell Biol. 11, 1287–1296.

Gibney, G.T., and Zager, J.S. (2013). Clinical development of dabrafenib in BRAF mutant melanoma and other malignancies. Expert Opin. Drug Metab. Toxicol. 9, 893–899.

Girotti, M.R., Lopes, F., Preece, N., Niculescu-Duvaz, D., Zambon, A., Davies, L., Whittaker, S., Saturno, G., Viros, A., Pedersen, M., et al. (2015). Paradox-breaking RAF inhibitors that also target SRC are effective in drug-resistant BRAF mutant melanoma. Cancer Cell 27, 85–96.

Harvey, C.D., Ehrhardt, A.G., Cellurale, C., Zhong, H., Yasuda, R., Davis, R.J., and Svoboda, K. (2008). A genetically encoded fluorescent sensor of ERK activity. Proc. Natl. Acad. Sci. USA 105, 19264–19269.

Hatzivassiliou, G., Song, K., Yen, I., Brandhuber, B.J., Anderson, D.J., Alvarado, R., Ludlam, M.J., Stokoe, D., Gloor, S.L., Vigers, G., et al. (2010). RAF inhibitors prime wild-type RAF to activate the MAPK pathway and enhance growth. Nature 464, 431–435.

Heidorn, S.J., Milagre, C., Whittaker, S., Nourry, A., Niculescu-Duvas, I., Dhomen, N., Hussain, J., Reis-Filho, J.S., Springer, C.J., Pritchard, C., and Marais, R. (2010). Kinase-dead BRAF and oncogenic RAS cooperate to drive tumor progression through CRAF. Cell 140, 209–221.

Huang, T., Karsy, M., Zhuge, J., Zhong, M., and Liu, D. (2013). B-Raf and the inhibitors: from bench to bedside. J Hematol Oncol 6, 30.

Inukai, M., Toyooka, S., Ito, S., Asano, H., Ichihara, S., Soh, J., Suehisa, H., Ouchida, M., Aoe, K., Aoe, M., et al. (2006). Presence of epidermal growth factor receptor gene T790M mutation as a minor clone in non-small cell lung cancer. Cancer Res. 66, 7854–7858.
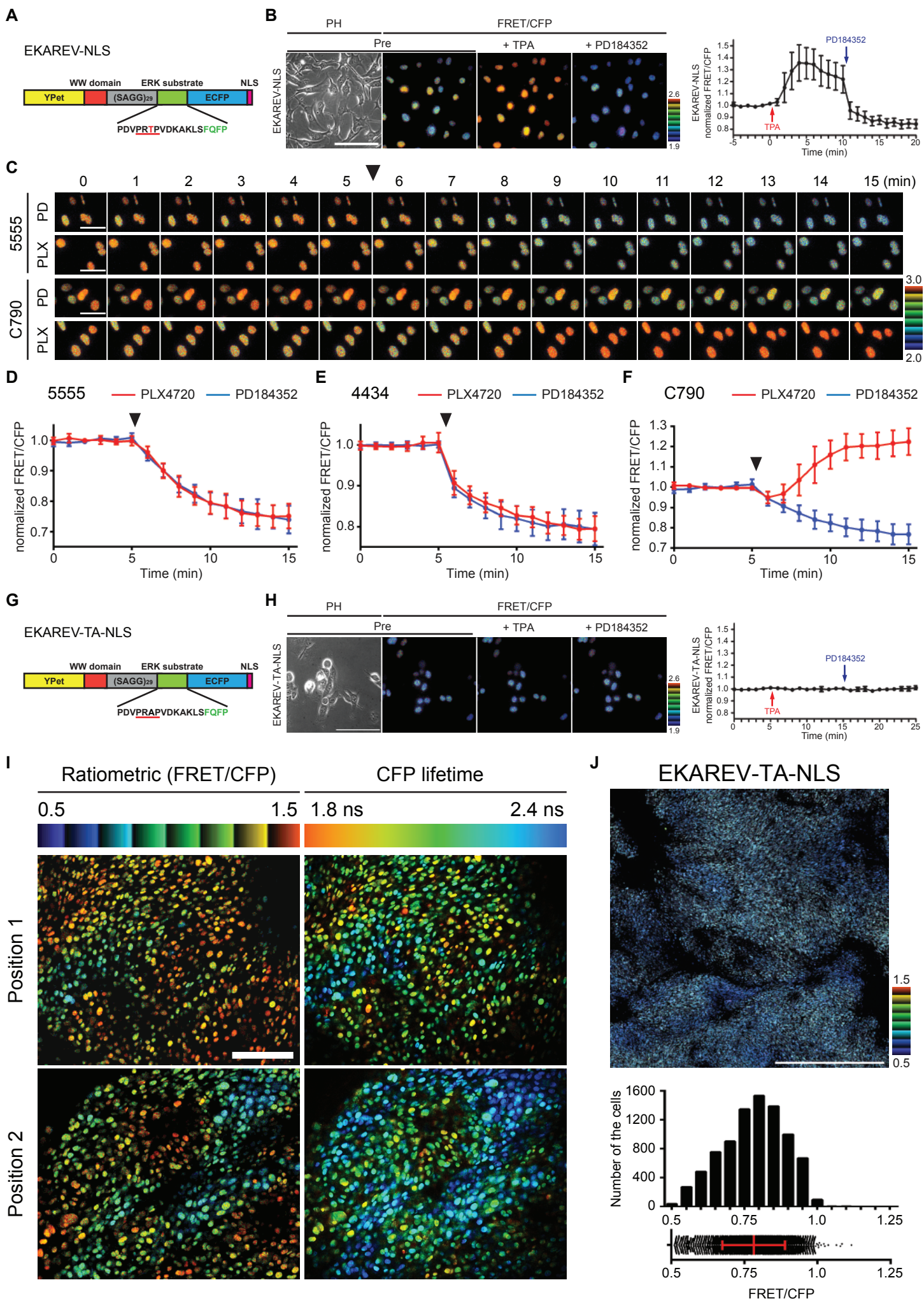
Janssen, A., Beerling, E., Medema, R., and van Rheenen, J. (2013). Intravital FRET imaging of tumor cell viability and mitosis during chemotherapy. PLoS ONE 8, e64029.

Kalluri, R., and Zeisberg, M. (2006). Fibroblasts in cancer. Nat. Rev. Cancer 6, 392–401.

Kobayashi, S., Boggon, T.J., Dayaram, T., Jänne, P.A., Kocher, O., Meyerson, M., Johnson, B.E., Eck, M.J., Tenen, D.G., and Halmos, B. (2005). EGFR mutation and resistance of non-small-cell lung cancer to gefitinib. N. Engl. J. Med. 352, 786–792.

Komatsu, N., Aoki, K., Yamada, M., Yukinaga, H., Fujita, Y., Kamioka, Y., and Matsuda, M. (2011). Development of an optimized backbone of FRET biosensors for kinases and GTPases. Mol. Biol. Cell 22, 4647–4656.

Larkin, J., Ascierto, P.A., Dréno, B., Atkinson, V., Liszkay, G., Maio, M., Mandalà, M., Demidov, L., Stroyakovskiy, D., Thomas, L., et al. (2014). Combined vemurafenib and cobimetinib in BRAF-mutated melanoma. N. Engl. J. Med. 371, 1867–1876.

Lito, P., Pratilas, C.A., Joseph, E.W., Tadi, M., Halilovic, E., Zubrowski, M., Huang, A., Wong, W.L., Callahan, M.K., Merghoub, T., et al. (2012). Relief of profound feedback inhibition of mitogenic signaling by RAF inhibitors attenuates their activity in BRAFV600E melanomas. Cancer Cell 22, 668–682.

Lito, P., Rosen, N., and Solit, D.B. (2013). Tumor adaptation and resistance to RAF inhibitors. Nat. Med. 19, 1401–1409.

Maemondo, M., Inoue, A., Kobayashi, K., Sugawara, S., Oizumi, S., Isobe, H., Gemma, A., Harada, M., Yoshizawa, H., Kinoshita, I., et al.; North-East Japan Study Group (2010). Gefitinib or chemotherapy for non-small-cell lung cancer with mutated EGFR. N. Engl. J. Med. 362, 2380–2388.

Maheswaran, S., Sequist, L.V., Nagrath, S., Ulkus, L., Brannigan, B., Collura, C.V., Inserra, E., Diederichs, S., Iafrate, A.J., Bell, D.W., et al. (2008). Detection of mutations in EGFR in circulating lung-cancer cells. N. Engl. J. Med. 359, 366–377.

Mok, T.S., Wu, Y.L., Thongprasert, S., Yang, C.H., Chu, D.T., Saijo, N., Sunpaweravong, P., Han, B., Margono, B., Ichinose, Y., et al. (2009). Gefitinib or carboplatin-paclitaxel in pulmonary adenocarcinoma. N. Engl. J. Med. 361, 947–957.

Muzumdar, M.D., Tasic, B., Miyamichi, K., Li, L., and Luo, L. (2007). A global double-fluorescent Cre reporter mouse. Genesis 45, 593–605.

Nazarian, R., Shi, H., Wang, Q., Kong, X., Koya, R.C., Lee, H., Chen, Z., Lee, M.K., Attar, N., Sazegar, H., et al. (2010). Melanomas acquire resistance to B-RAF(V600E) inhibition by RTK or N-RAS upregulation. Nature 468, 973–977.

Paszek, M.J., Zahir, N., Johnson, K.R., Lakins, J.N., Rozenberg, G.I., Gefen, A., Reinhart-King, C.A., Margulies, S.S., Dembo, M., Boettiger, D., et al. (2005). Tensional homeostasis and the malignant phenotype. Cancer Cell 8, 241–254.

Pedersen, M., Kusters-Vandevelde, H.V., Viros, A., Groenen, P.J., Sanchez-Laorden, B., Gilhuis, J.H., van Engen-van Grunsven, I.A., Renier, W., Schieving, J., Niculescu-Duvaz, I., et al. (2013). Primary melanoma of the CNS in children is driven by congenital expression of oncogenic NRAS in melanocytes. Cancer Discov 3, 458–469.

Pietras, K., Pahler, J., Bergers, G., and Hanahan, D. (2008). Functions of paracrine PDGF signaling in the proangiogenic tumor stroma revealed by pharmacological targeting. PLoS Med. 5, e19.

Poulikakos, P.I., and Rosen, N. (2011). Mutant BRAF melanomas—dependence and resistance. Cancer Cell 19, 11–15.

Poulikakos, P.I., Zhang, C., Bollag, G., Shokat, K.M., and Rosen, N. (2010). RAF inhibitors transactivate RAF dimers and ERK signalling in cells with wild-type BRAF. Nature 464, 427–430.

Poulikakos, P.I., Persaud, Y., Janakiraman, M., Kong, X., Ng, C., Moriceau, G., Shi, H., Atefi, M., Titz, B., Gabay, M.T., et al. (2011). RAF inhibitor resistance is mediated by dimerization of aberrantly spliced BRAF(V600E). Nature 480, 387–390.

Rosell, R., Molina, M.A., Costa, C., Simonetti, S., Gimenez-Capitan, A., Bertran-Alamillo, J., Mayo, C., Moran, T., Mendez, P., Cardenal, F., et al. (2011). Pretreatment EGFR T790M mutation and BRCA1 mRNA expression in erlotinib-treated advanced non-small-cell lung cancer patients with EGFR mutations. Clin. Cancer Res. 17, 1160–1168.

Shawver, L.K., Slamon, D., and Ullrich, A. (2002). Smart drugs: tyrosine kinase inhibitors in cancer therapy. Cancer Cell 1, 117–123.

Shi, H., Hugo, W., Kong, X., Hong, A., Koya, R.C., Moriceau, G., Chodon, T., Guo, R., Johnson, D.B., Dahlman, K.B., et al. (2014). Acquired resistance and clonal evolution in melanoma during BRAF inhibitor therapy. Cancer Discov 4, 80–93.

Sordella, R., Bell, D.W., Haber, D.A., and Settleman, J. (2004). Gefitinib-sensitizing EGFR mutations in lung cancer activate anti-apoptotic pathways. Science 305, 1163–1167.

Sosman, J.A., Kim, K.B., Schuchter, L., Gonzalez, R., Pavlick, A.C., Weber, J.S., McArthur, G.A., Hutson, T.E., Moschos, S.J., Flaherty, K.T., et al. (2012). Survival in BRAF V600-mutant advanced melanoma treated with vemurafenib. N. Engl. J. Med. 366, 707–714.

Straussman, R., Morikawa, T., Shee, K., Barzily-Rokni, M., Qian, Z.R., Du, J., Davis, A., Mongare, M.M., Gould, J., Frederick, D.T., et al. (2012). Tumour micro-environment elicits innate resistance to RAF inhibitors through HGF secretion. Nature 487, 500–504.

Sulzmaier, F.J., Jean, C., and Schlaepfer, D.D. (2014). FAK in cancer: mechanistic findings and clinical applications. Nat. Rev. Cancer 14, 598–610.

Turke, A.B., Zejnullahu, K., Wu, Y.L., Song, Y., Dias-Santagata, D., Lifshits, E., Toschi, L., Rogers, A., Mok, T., Sequist, L., et al. (2010). Preexistence and clonal selection of MET amplification in EGFR mutant NSCLC. Cancer Cell 17, 77–88.

Van Allen, E.M., Wagle, N., Sucker, A., Treacy, D.J., Johannessen, C.M., Goetz, E.M., Place, C.S., Taylor-Weiner, A., Whittaker, S., Kryukov, G.V., et al.; Dermatologic Cooperative Oncology Group of Germany (DeCOG) (2014). The genetic landscape of clinical resistance to RAF inhibition in metastatic melanoma. Cancer Discov 4, 94–109.

Villanueva, J., Vultur, A., Lee, J.T., Somasundaram, R., Fukunaga-Kalabis, M., Cipolla, A.K., Wubbenhorst, B., Xu, X., Gimotty, P.A., Kee, D., et al. (2010). Acquired resistance to BRAF inhibitors mediated by a RAF kinase switch in melanoma can be overcome by cotargeting MEK and IGF-1R/PI3K. Cancer Cell 18, 683–695.

Villanueva, J., Vultur, A., and Herlyn, M. (2011). Resistance to BRAF inhibitors: unraveling mechanisms and future treatment options. Cancer Res. 71, 7137–7140.

Wagle, N., Van Allen, E.M., Treacy, D.J., Frederick, D.T., Cooper, Z.A., Taylor-Weiner, A., Rosenberg, M., Goetz, E.M., Sullivan, R.J., Farlow, D.N., et al. (2014). MAP kinase pathway alterations in BRAF-mutant melanoma patients with acquired resistance to combined RAF/MEK inhibition. Cancer Discov 4, 61–68.

Watson, I.R., Li, L., Cabeceiras, P.K., Mahdavi, M., Gutschner, T., Genovese, G., Wang, G., Fang, Z., Tepper, J.M., Stemke-Hale, K., et al. (2014). The RAC1 P29S hotspot mutation in melanoma confers resistance to pharmacological inhibition of RAF. Cancer Res. 74, 4845–4852.

Wilson, T.R., Fridlyand, J., Yan, Y., Penuel, E., Burton, L., Chan, E., Peng, J., Lin, E., Wang, Y., Sosman, J., et al. (2012). Widespread potential for growth-factor-driven resistance to anticancer kinase inhibitors. Nature 487, 505–509.

Supplemental Information

Intravital Imaging Reveals How BRAF Inhibition

Generates Drug-Tolerant Microenvironments

with High Integrin β1/FAK Signaling

Eishu Hirata, Maria Romina Girotti, Amaya Viros, Steven Hooper, Bradley Spencer-Dene, Michiyuki Matsuda, James Larkin, Richard Marais, and Erik Sahai
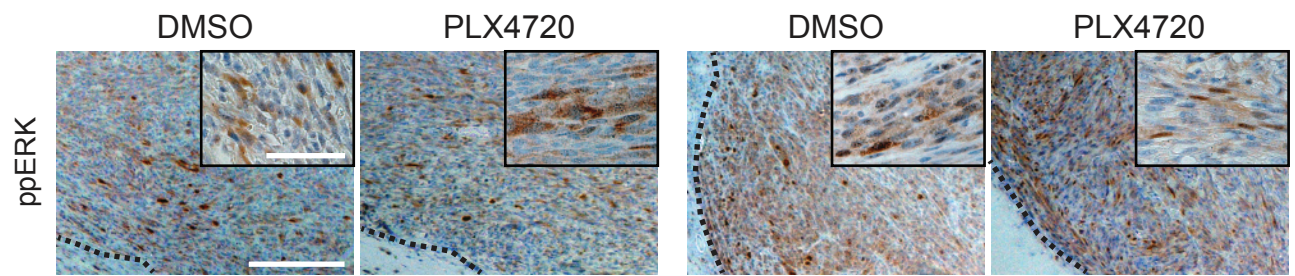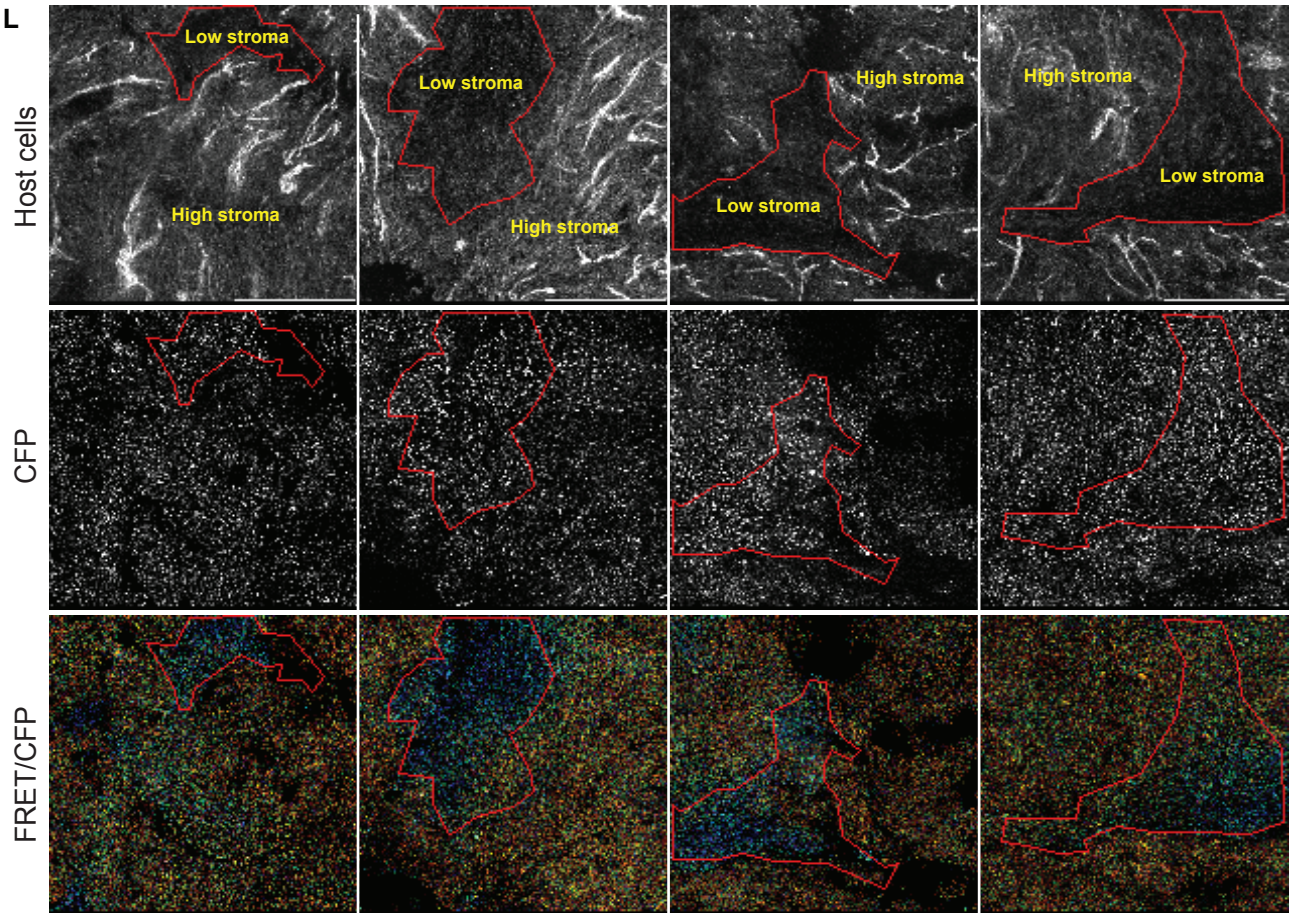
A EKAREV-NLS
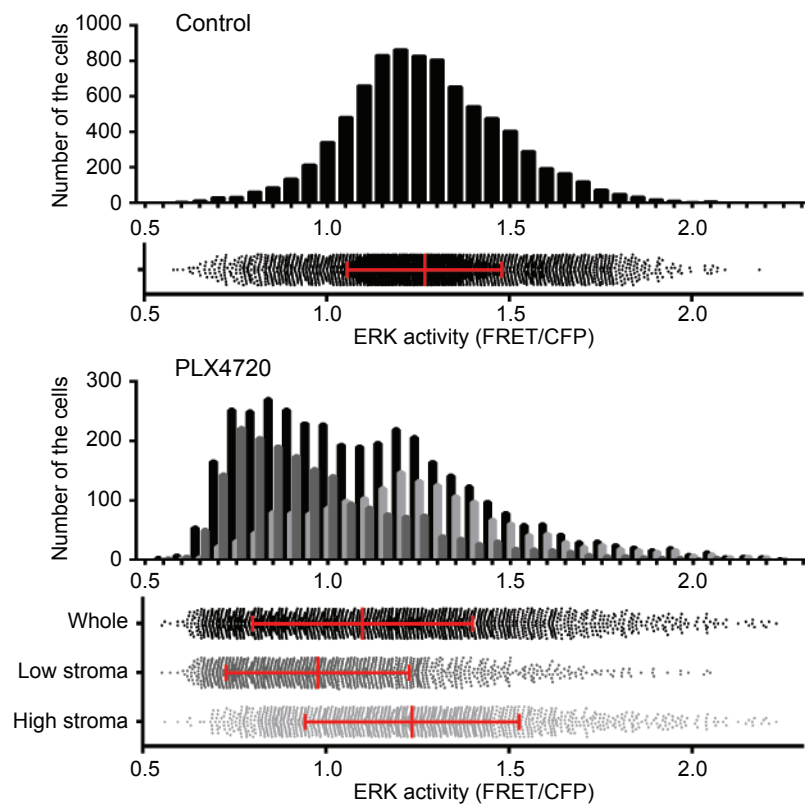
B

C

D 5555

E 4434

F C790

G EKAREV-TA-NLS

H

I Ratiometric (FRET/CFP)   CFP lifetime

J EKAREV-TA-NLS

K

	5555		4434	
ppERK	DMSO	PLX4720	DMSO	PLX4720

L

Host cells

Low stroma / High stroma

CFP

FRET/CFP

M

4434-EKAREV-NLS

Control

Number of the cells

ERK activity (FRET/CFP)

PLX4720

Number of the cells

Whole
Low stroma
High stroma

ERK activity (FRET/CFP)

Figure S1. (Related to Figure 1.) Intravital FRET imaging revealed heterogeneous response to a BRAF inhibitor, which is related to stromal cell density.

(A) A scheme of EKAREV-NLS biosensor. (B) B16F10 mouse melanoma cells expressing EKAREV-NLS biosensors were treated with 12-O-Tetradcanoyl-phorbol-13-acetate (TPA) (100 nM) and PD184352 (1 μM) at the indicated time points. Images are acquired every 1 min and normalized FRET/CFP ratios were quantified and shown as mean ± SD (n = 10). Scale bar = 100 μm. (C-F) Indicated cells expressing EKAREV-NLS were treated with 1 μM PLX4720 (quantified in red curves) or 1 μM PD184352 (in blue curves) at time = 5 min (indicated by arrowheads). Normalized ERK activities (FRET/CFP) are shown as mean ± SD. Scale bars = 50 μm. (G) A scheme of negative control ERK biosensor (EKAREV-TA-NLS). (H) B16F10 mouse melanoma cells expressing EKAREV-TA-NLS biosensors were treated with TPA (100 nM) and PD184352 (1 μM) at the indicated time points. Images are acquired every 1 min and normalized FRET/CFP ratios were quantified and shown as mean ± SD (n = 10). Scale bar = 100 μm. (I) Same positions of 5555-EKAREV-NLS tumors in C57BL/6 mice were successively imaged and analyzed by intensity-based ratiometric analysis (FRET/CFP) (left panels) and time-correlated single photon counting (TCSPC) FLIM-FRET analysis (right panels). Scale bar = 100 μm. (J) A representative image of 5555-EKAREV-TA-NLS grown subcutaneously in a C57BL/6 mouse, and the distribution (a scatter plot with mean ± SD) and histogram of FRET/CFP are quantified and shown. Scale bar = 500 μm. (K) 5555 and 4434 allografts treated with DMSO (4%) or PLX4720 (25 mg/kg) for 8-14 days were fixed and stained with a phosphor-ERK antibody. Tumor margins are delineated by dashed lines, and enlarged views are also shown as insets. Scale bar = 200 μm and 50 μm (inset). (L) To quantify ERK activity in melanoma cells separately according to the surrounding stromal cell density, we manually set up ROIs depending on the intensity of mTomato (host cells) and defined 'low stroma' region (inside the red line in each panel) and 'high stroma' region (outside the red line). Scale bar = 500 μm.

(M) Quantification of ERK activity in skin-flap imaging of 4434-EKAREV-NLS in C57BL/6_ROSA26-mTmG mice, presented in the same manner as in Figure 1F.

A

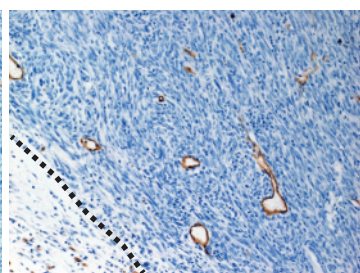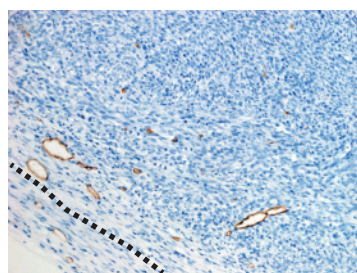|	5555		4434	
	DMSO	PLX4720	DMSO	PLX4720

αSMA
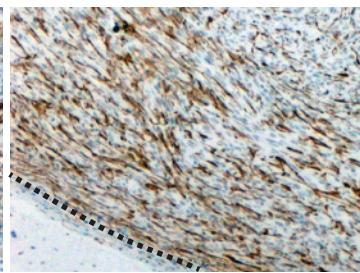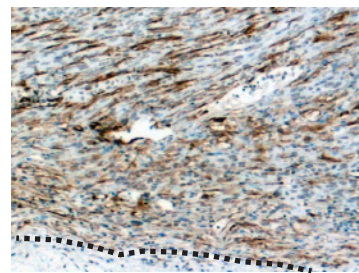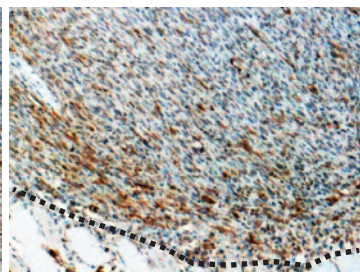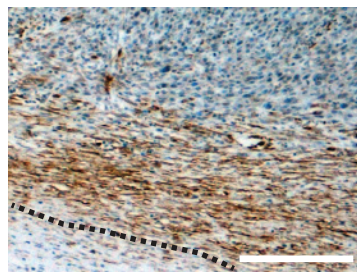
F4/80
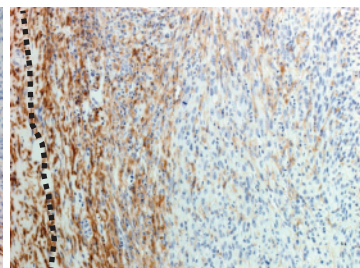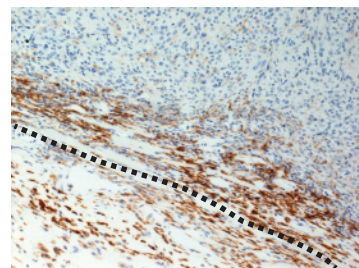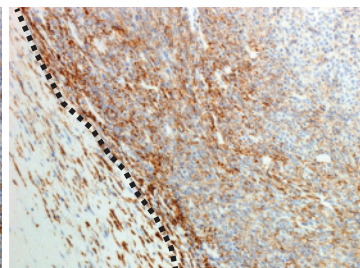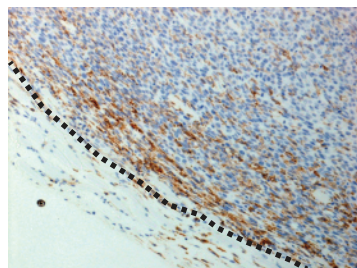
S100A9 (2B10)

CD3

Endomucin
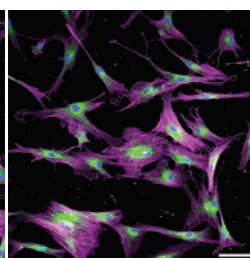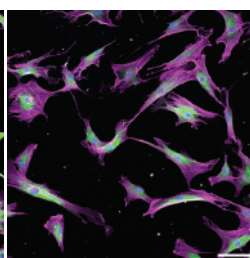
B
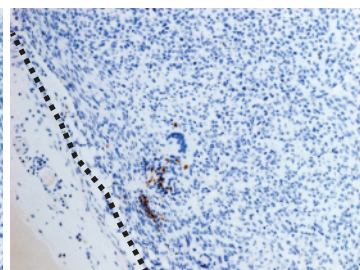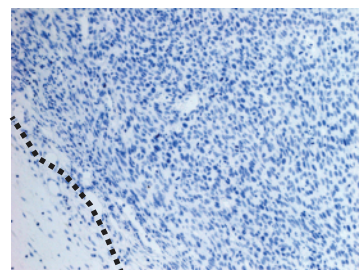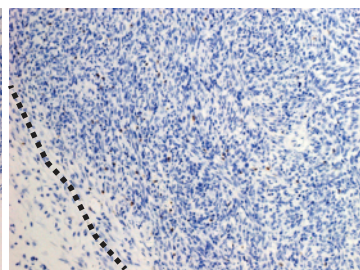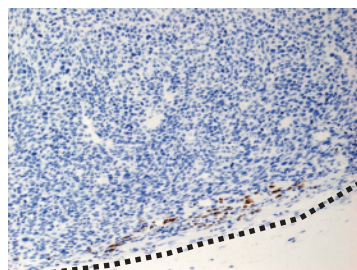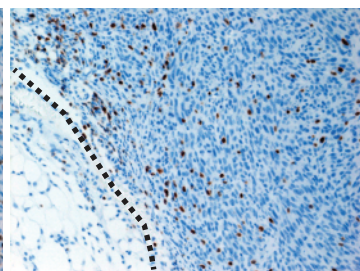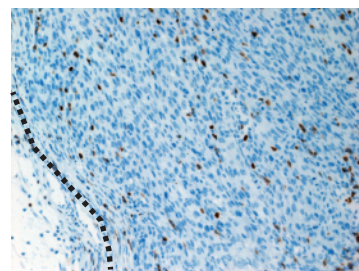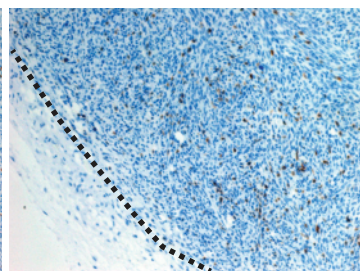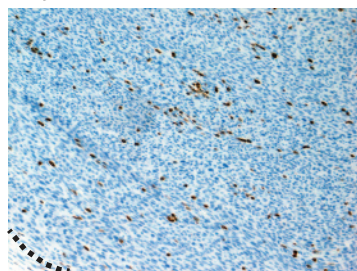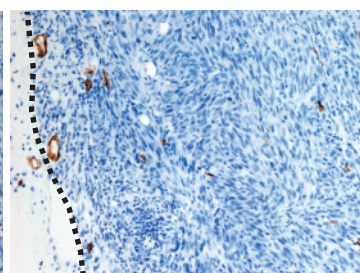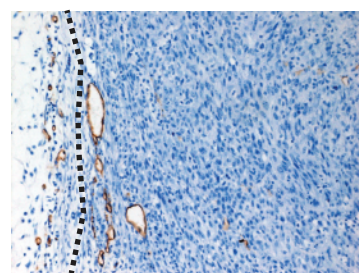
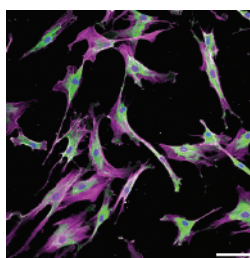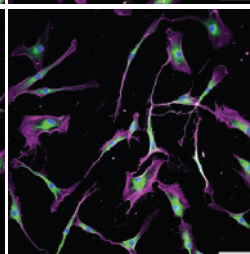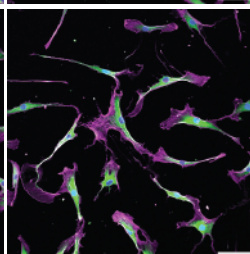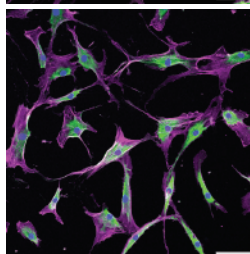|	H&E	αSMA
Melanoma tissue for MAF1		
Melanoma tissue for MAF2		
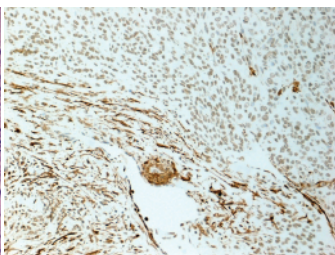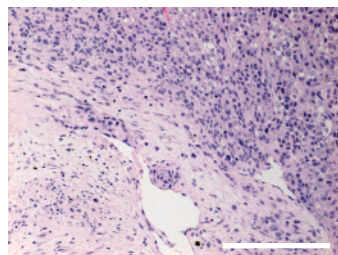
C
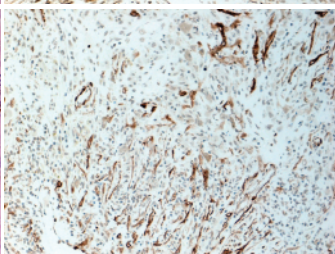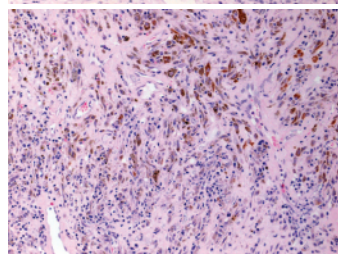
αSMA / Phalloidin / DAPI   S100A4 / Phalloidin / DAPI   FAP / Phalloidin / DAPI
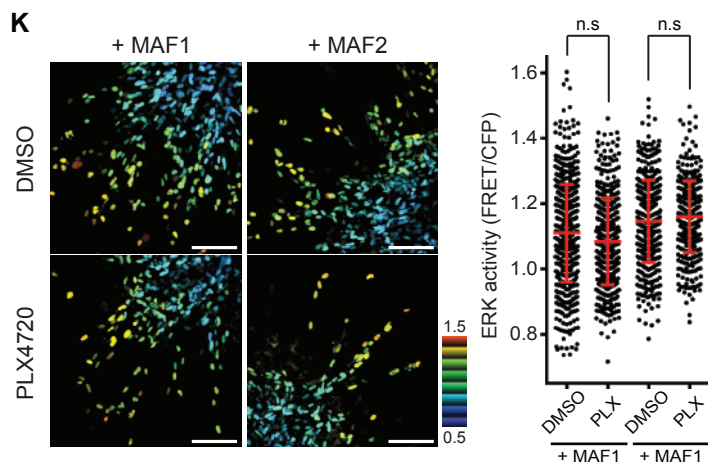
MAF1

MAF2

D

Spheroid | + MAF1 | + MAF2

DMSO / PLX4720

E

Mono | + MAF1-CM | + MAF1

DMSO / PLX4720

F

Mono | + MAF1-CM | + MAF1

DMSO / PLX4720

G

H

I

5555 | 5555 + BAC

DMSO / PLX4720

J

Explant | +MAF2

DMSO / PLX4720

K

+ MAF1 | + MAF2
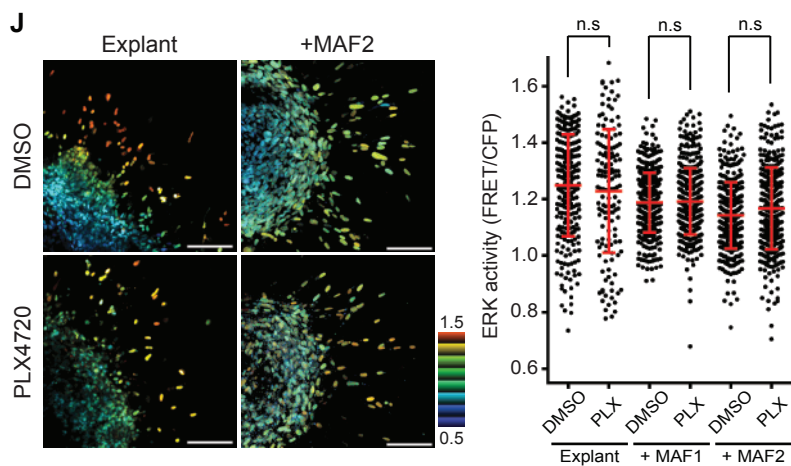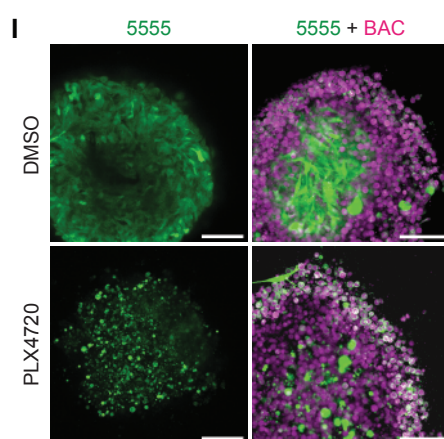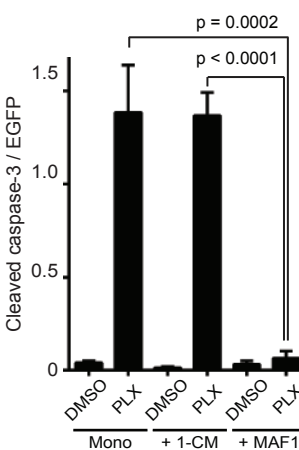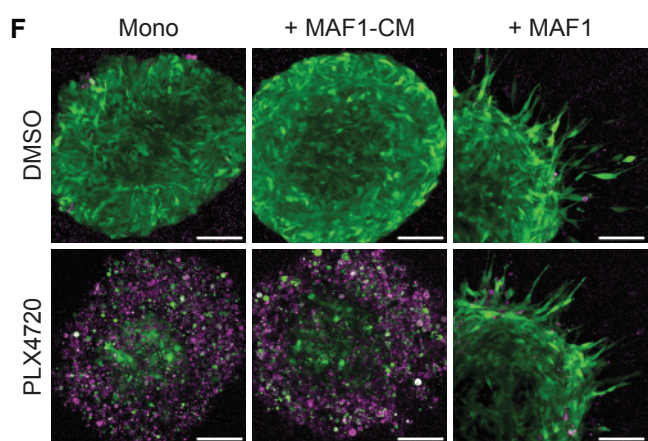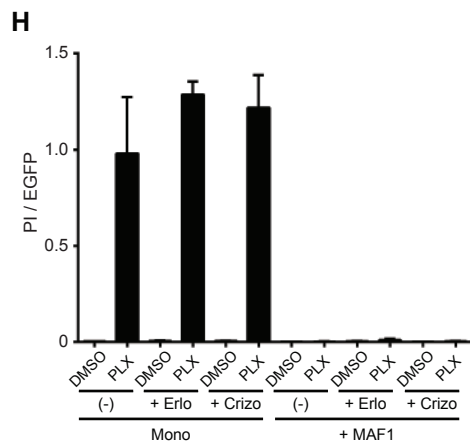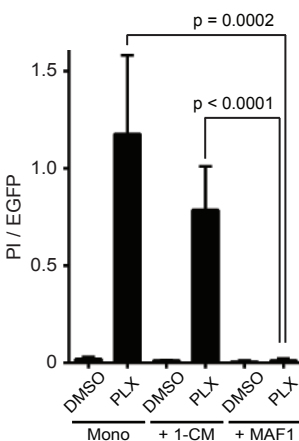
DMSO / PLX4720

Figure S2. (Related to Figure 2.) Melanoma-associated fibroblastg UY sufficient to induce ERK re-activation and drug tolerance.

(A) 5555 and 4434 allografts treated with DMSO (4%) or PLX4720 (25 mg/kg) for 8-14 days were fixed and stained with the indicated antibodies. Tumor margins are delineated by dashed lines. Scale bar = 200 μm. (B) Two human melanoma surgical specimens stained with H&E and anti-αSMA antibody. Scale bar = 200 μm. (C) Established MAFs cultured in DMEM are stained with the indicated antibodies. Scale bars = 100 μm. (D) 4434 (green) mono-cultured spheroids or co-cultured spheroids with MAF1/2 (magenta) were cultured in the same manner in Figure 2A, and the cell death was quantified in the same manner in Figure 2B. Scale bars = 100 μm. (E) 5555-mEGFP spheroids cultured with or without MAF1-conditioned media were treated with DMSO (0.1%) or PLX4720 (1 μM) for 24 hr, followed by propidium iodide (PI) staining. PI intensities were quantified and shown as mean ± SD. Scale bar = 100 μm. (F) 5555-mEGFP and MAF1 co-cultured spheroids were treated with DMSO (0.1%) or PLX4720 (1 μM) for 24 hr, fixed and stained with an anti-cleaved caspase-3 antibody. Cleaved caspase-3 signals were quantified and shown as mean ± SD. Scale bars = 100 μm. (G) 5555 and MAF1 co-cultured spheroids were treated with DMSO (0.1%), PLX4720 (1 μM), erlotinib (1 μM), crizotinib (1 μM) or the combination. Cell death was quantified by the ratio of DAPI-p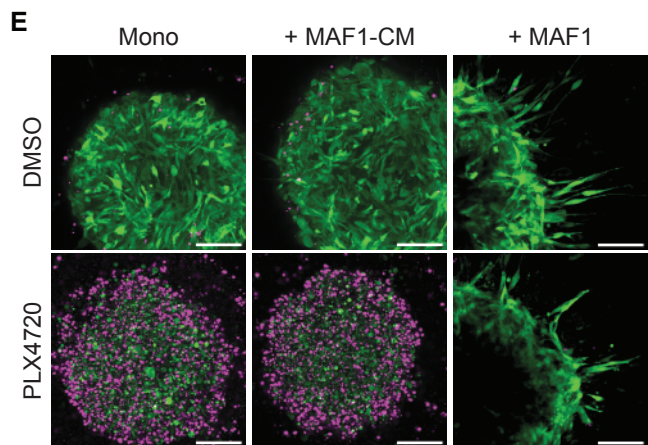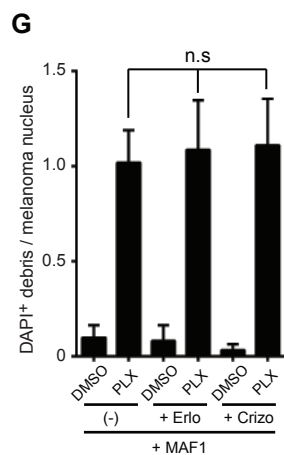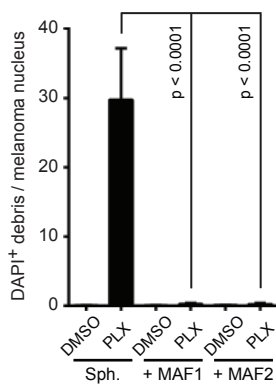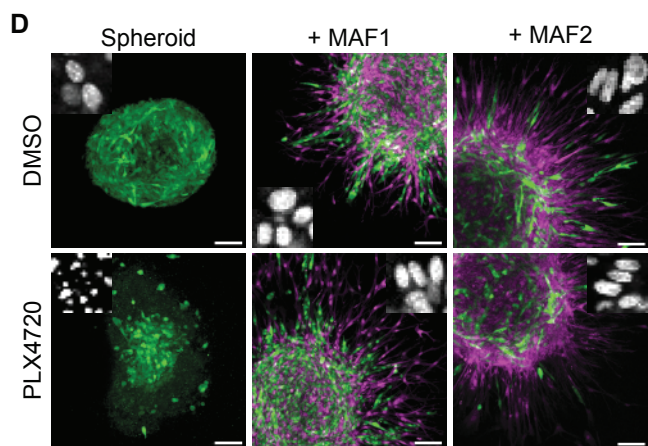ositive debris and 5555 nucleus. (mean ± SD). (H) 5555 mono-cultured spheroids or 5555 and MAF1 co-cultured spheroids were treated with DMSO (0.1%), PLX4720 (1 μM), erlotinib (1 μM), crizotinib (1 μM) or the combination. Cell death was quantified by PI staining (mean ± SD). (I) 5555-mEGFP (in green) mono-cultured spheroids or co-cultured spheroids with BAC macrophage cells (labeled with Cherry and shown in magenta) were treated with DMSO (0.1%) or PLX4720 (1 μM) for 24 hr. Scale bars = 100 μm. (J) 5555-EKAREV-NLS tumor explants or co-cultured spheroids with MAF1/2 were embedded into collagen gels and treated with DMSO (0.1%) or PLX4720 (1 μM) for 24 hr. ERK activity in invaded 5555 cells were quantified and shown as scatter plots with mean ± SD. Scale bars = 100 μm. (K) 4434-EKAREV-NLS and MAF1/2-

mCherry co-cultured spheroids were treated in the same manner in (J) and ERK activities were quantified and shown in the same manner in (J). Scale bars = 100 μm.

Movie S1. (Related to Figure 2.) Melanoma-associated fibroblasts provide invasive and pro-survival signals, and the system adapts to the drug within 12 hr.

5555-EKAREV-NLS mono-cultured spheroids (Mono) or co-cultured spheroids with MAF1-mCherry (+ MAF1) were embedded in collagen gels and treated with DMSO (0.1%) or PLX4720 (1 μM). Images were acquired every 5 min for 13 hr. Scale bars = 100 μm.

A

B

C

D
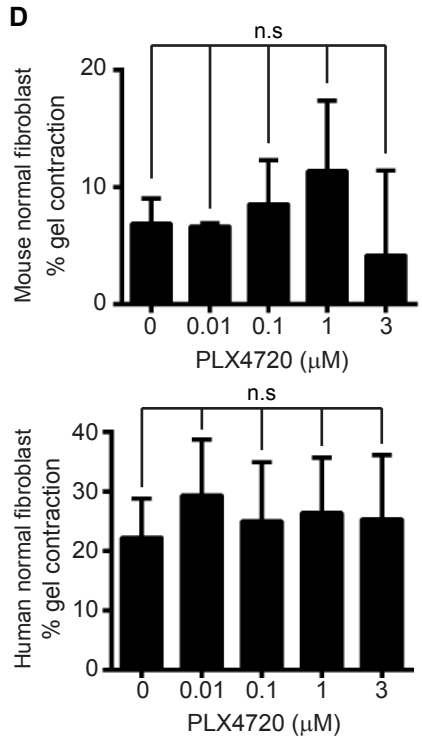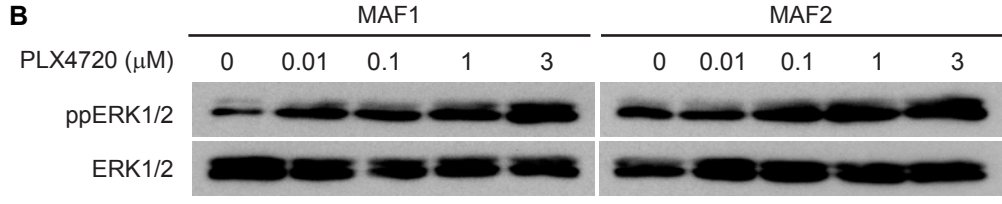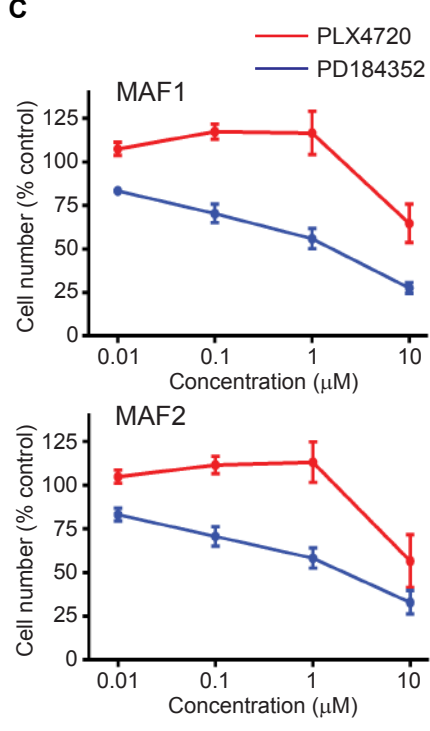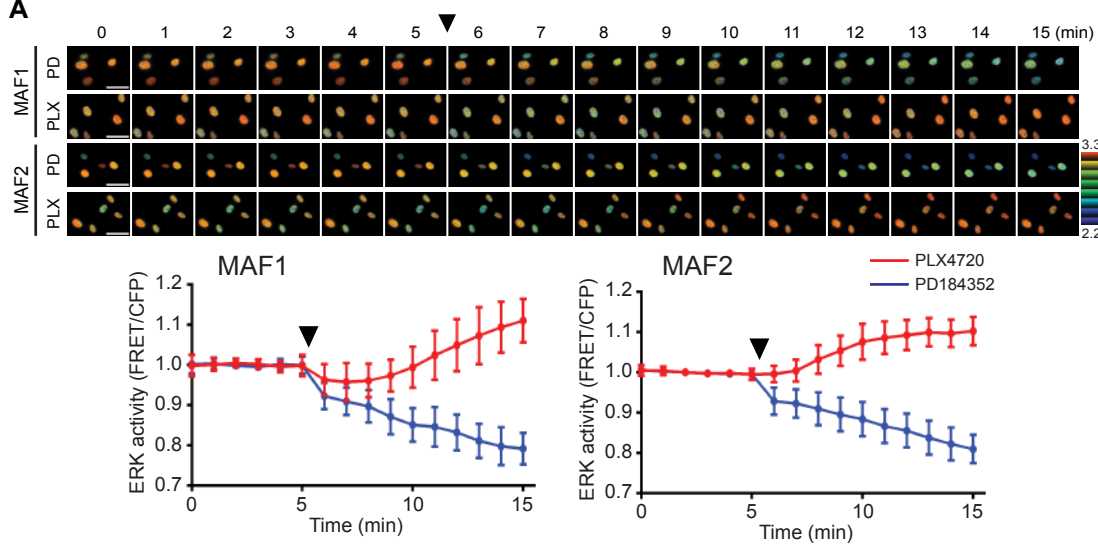
E

Matrix components	
THBS1	1.995870283
THBS2	1.545994653
LUM	1.479525545
POSTN	1.476500263
COL12A1	1.43913
LAMB1	1.410675
COL4A1	1.353
TNC	1.233553
FN1	1.163538

Soluble factors	
HGF	1.04796
IGF1	1.037288
HBEGF	1.056623221
EGF	0.995187566

Receptor Tyrosine Kinases	
PDGFRA	1.496068778
PDGFRB	1.016803791

F

Proteinaceous_Extracellular_Matrix
(GO 0005578)
NES = 1.57   p value = 0.005

Extracellular_Matrix
(GO 0031012)
NES = 1.56   p value = 0.005

G

Figure S3. (Related to Figure 3.) PLX4720 paradoxically activates MAFs and induces ECM expression.

(A) Timelapse images of MAF1/2 -EKAREV-NLS, stimulated with PLX4720 (1 μM) or PD184352 (1 μM) at time = 5 min (indicated by arrowheads). ERK activities in MAF1 and MAF2 were quantified and shown as normalized FRET/CFP ratio (n = 10, mean ± SD). Scale bars = 50 μm. (B) Immunoblotting for the indicated proteins in MAF1/2 treated with different concentration of PLX4720 (0–3 μM). (C) Cell viability assay of MAF1 and MAF2 treated with different concentration of PLX4720 (red curves) and PD184352 (blue curves) for 3 days. Data are represented as mean ± SD. (D) Histograms of gel contraction by mouse lung normal fibroblasts and human dermal normal fibroblasts treated with different concentration of PLX4720 (0–3 μM). Data are represented as mean ± SD. (E) 5555-mEGFP and MAF2-mCherry were co-cultured and treated with DMSO (0.1%) or PLX4720 (1 μM) for 24 hr. Cells were trypsinized, sorted according to the expression of EGFP and Cherry, and total RNA was extracted from each component. Gene expression was analyzed with a microarray and the fold change (up-regulated in PLX4720-treated MAF2 compared to DMSO-treated MAF2) of matrix components, soluble factors, and receptor tyrosine kinases of our interest are shown. More details are available as Table S1. (F) Gene set enrichment analysis of PLX4720-treated MAF2 versus DMSO-treated MAF2 with the indicated data sets. (G) Histograms of MAF1 and MAF2 gel contraction with DMSO (0.1%), imatinib (1 μM), sunitinib (1 μM) ± PLX4720 (1 μM) from 3 independent experiments (mean ± SD).

Movie S2. (Related to Figure 3.) PLX4720 paradoxically activate ERK in MAFs.

5555-EKAREV-NLS and MAF1-EKAREV-NLS-mCherry co-cultured spheroids were embedded in collagen gels and treated with PLX4720 (1 μM). Images were acquired every 5 min for 13 hr. White arrows indicate MAF nuclei to be focused on. Scale bars = 100 μm.

Movie S3. (Related to Figure 3.) PLX4720 promotes MAF motility and elongation.

MAF1/2-mCherry embedded in collagen/Matrigel with 10%FBS were treated with DMSO (0.1%) or PLX4720 (1 μM). Images were acquired every 10 min for 13 hr. Scale bars = 100 μm.

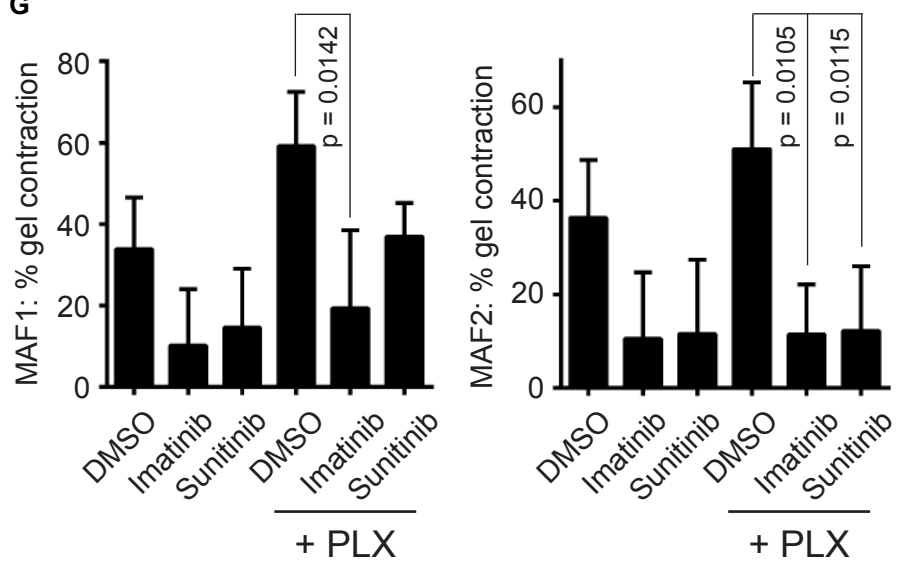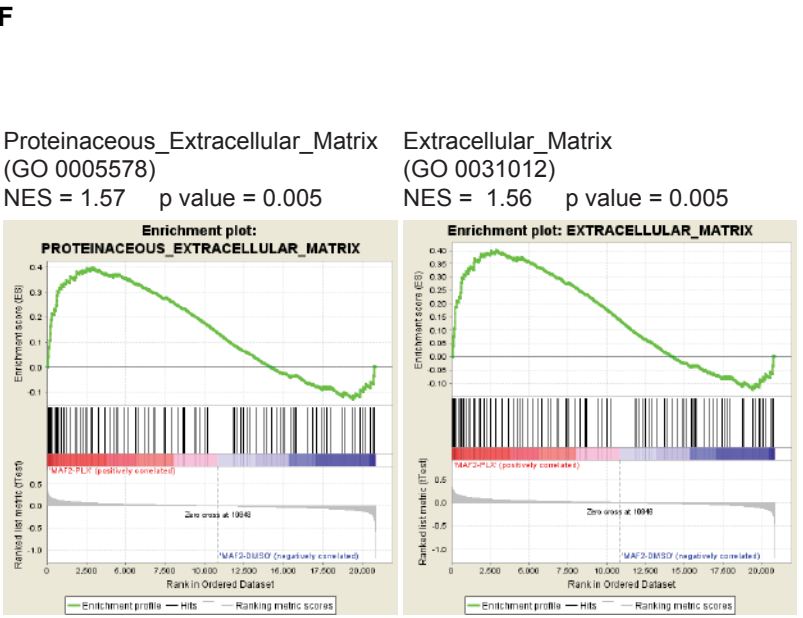**Table S1. (Related to Figure 3. Provided as an Excel file.) Summary of the microarray.**

A

5555

x 10E6

DMSO PLX

(-)
FN
CTGF
TNC
THBS1
THBS2 THBS1
POSTN THBS2

P = 0.0118

P = 0.0004

Relative intensity

(19.3 ± 3.1)
(43.1 ± 3.0)
(29.1 ± 2.2)
(36.3 ± 5.4)
(27.4 ± 5.7)
(34.0 ± 15.8)
(26.6 ± 8.3)

D P D P D P D P D P D P D P
(-) FN CTGF TNC THBS1 THBS2 POSTN

4434

x 10E5

DMSO PLX

(-)
FN
CTGF
TNC
THBS1
THBS2 THBS1
POSTN THBS2

P = 0.0033

P = 0.0074

P = 0.0033

Relative intensity

(43.7 ± 10.0)
(75.1 ± 10.4)
(80.7 ± 5.7)
(69.5 ± 18.5)
(110.0 ± 51.9)
(87.9 ± 36.6)
(66.3 ± 53.4)

D P D P D P D P D P D P D P
(-) FN CTGF TNC THBS1 THBS2 POSTN

B

0.2 kPa   3 kPa   12 kPa

Integrin β1 / DAPI

C

DMSO   PLX4720

4434 (+ MAF1)   Integrin β1 / pFAK

D

5555   4434

si-Ctrl si-β1 si-FAK si-Ctrl si-β1 si-FAK

pFAK

FAK

Tubulin

E

Before   + 30 min   + 4 hr   + 12 hr

si-Ctrl

5555 (Cherry)

ERK activity

si-Integrin β1

5555 (Cherry)

ERK activity

si-FAK

5555 (Cherry)

ERK activity

1.5

0.5

Figure S4. (Related to Figure 4.) ECM provides drug tolerant microenvironment through integrin β1-FAK signaling.

(A) 5555 and 4434 cells expressing firefly luciferase were seeded onto 96-well plate coated with collagen I (100 mg/ml) ± fibronectin (20 mg/ml), CTGF (20 mg/ml), tenascin-C (20 mg/ml), thrombospondin-1 (20 mg/ml), thrombospondin-2 (20 mg/ml), or periostin (20 mg/ml), and treated with DMSO (0.1%) or PLX4720 (1 μM) for 24 hr, followed by bioluminescence imaging. Signals were quantified and shown in the graphs (n = 3, mean ± SD). (B) 5555 cells cultured on the fibronectin-coated gels with the indicated stiffness were fixed and stained with an anti-active integrin β1 antibody (9EG7) (in green) and DAPI (in magenta). Scale bars = 50 μm. (C) 4434 cells (blue) were co-cultured with MAF1 (not labeled) and treated with DMSO (0.1%) or PLX4720 (1 μM) for 24 hr. After fixation, cells were double-stained with an anti-active integrin β1 antibody (9EG7) (red) and an anti-phospho-FAK antibody (green). Scale bars = 20 μm. (D) Immunoblotting for the indicated proteins in 5555 and 4434 cells transfected with the indicated siRNAs. (E) 5555-EKAREV-NLS-mCherry transfected with the indicated siRNAs were seeded onto collagen gels with MAF1 (not labeled) and imaged before and after PLX4720 treatment. Scale bars = 100 μm.
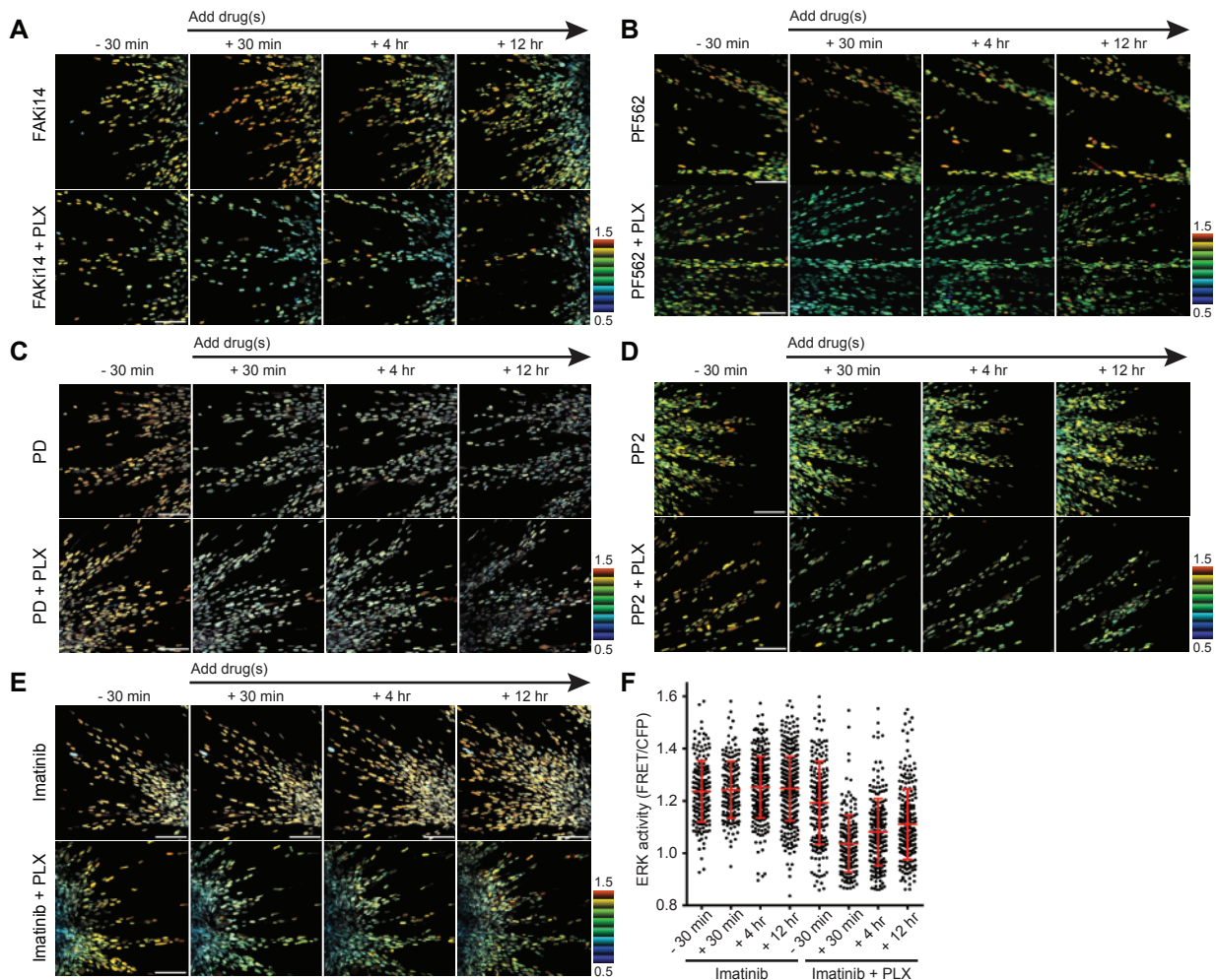
G		DMSO		PLX4720	
(-)	p = 0.1022	Before: 1.180 ± 0.010, n=238	p = 0.1006	Before: 1.176 ± 0.010, n=189
		12 hr: 1.203 ± 0.010, n=279		12 hr: 1.152 ± 0.011, n=200
		ND: 1.019 ± 0.008		ND: 0.982 ± 0.009
Imatinib	p = 0.3255	Before: 1.236 ± 0.009, n=187	p < 0.0001	Before: 1.192 ± 0.014, n=196
		12 hr: 1.247 ± 0.006, n=385		12 hr: 1.111 ± 0.009, n=248
		ND: 1.008 ± 0.005		ND: 0.931 ± 0.007
PF573228	p = 0.0099	Before: 1.205 ± 0.009, n=160	p < 0.0001	Before: 1.167 ± 0.007, n=199
		12 hr: 1.172 ± 0.009, n=130		12 hr: 1.057 ± 0.018, n=62
		ND: 0.973 ± 0.008		ND: 0.906 ± 0.015
PF562271	p = 0.0270	Before: 1.237 ± 0.009, n=138	p < 0.0001	Before: 1.176 ± 0.007, n=172
		12 hr: 1.266 ± 0.009, n=114		12 hr: 1.120 ± 0.008, n=123
		ND: 1.023 ± 0.007		ND: 0.949 ± 0.006
FAK inhibitor 14	p = 0.4734	Before: 1.181 ± 0.007, n=185	p < 0.0001	Before: 1.143 ± 0.009, n=168
		12 hr: 1.188 ± 0.008, n=194		12 hr: 1.033 ± 0.016, n=75
		ND: 1.006 ± 0.006		ND: 0.903 ± 0.014
Dasatinib	p < 0.0001	Before: 1.186 ± 0.005, n=243	p < 0.0001	Before: 1.221 ± 0.008, n=188
		12 hr: 1.136 ± 0.005, n=288		12 hr: 1.000 ± 0.006, n=277
		ND: 0.958 ± 0.004		ND: 0.819 ± 0.005
PP2	p = 0.1988	Before: 1.160 ± 0.011, n=115	p < 0.0001	Before: 1.186 ± 0.009, n=129
		12 hr: 1.179 ± 0.010, n=179		12 hr: 0.990 ± 0.006, n=134
		ND: 1.016 ± 0.009		ND: 0.835 ± 0.005
PD184352	p < 0.0001	Before: 1.233 ± 0.007 n=237	p < 0.0001	Before: 1.218 ± 0.008, n=236
		12 hr: 0.965 ± 0.004, n=260		12 hr: 0.998 ± 0.006, n=233
		ND: 0.783 ± 0.004		ND: 0.801 ± 0.004

H
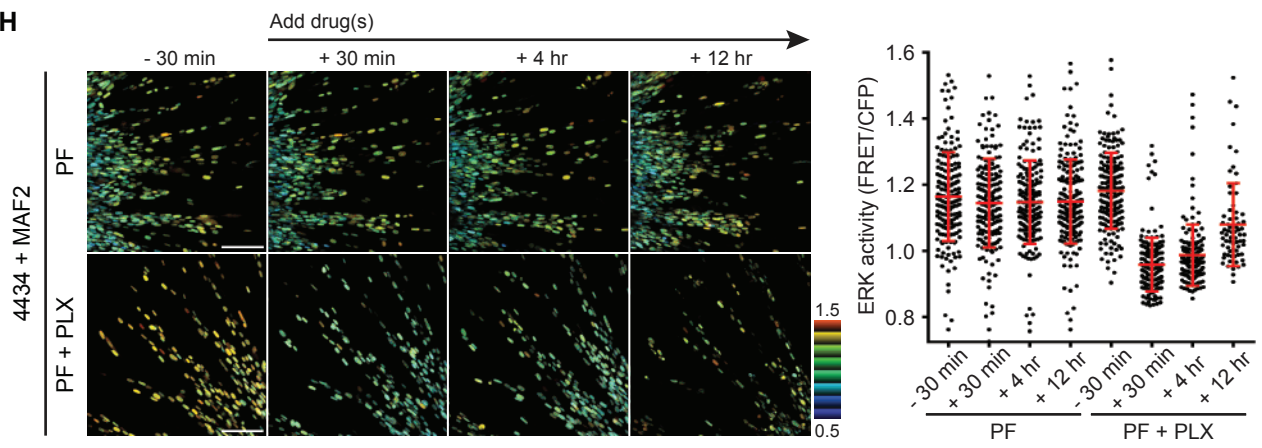
I

	DMSO		PLX4720	
(-)	NA		p = 0.2363	Before: 1.075 ± 0.123, n=225 12 hr: 1.061 ± 0.117, n=201 ND: 0.987 ± 0.108
PF573228	p = 0.2698	Before: 1.164 ± 0.134, n=185 12 hr: 1.149 ± 0.127, n=206 ND: 0.987 ± 0.109	p < 0.0001	Before: 1.182 ± 0.115, n=182 12 hr: 1.079 ± 0.126, n=70 ND: 0.913 ± 0.106

J
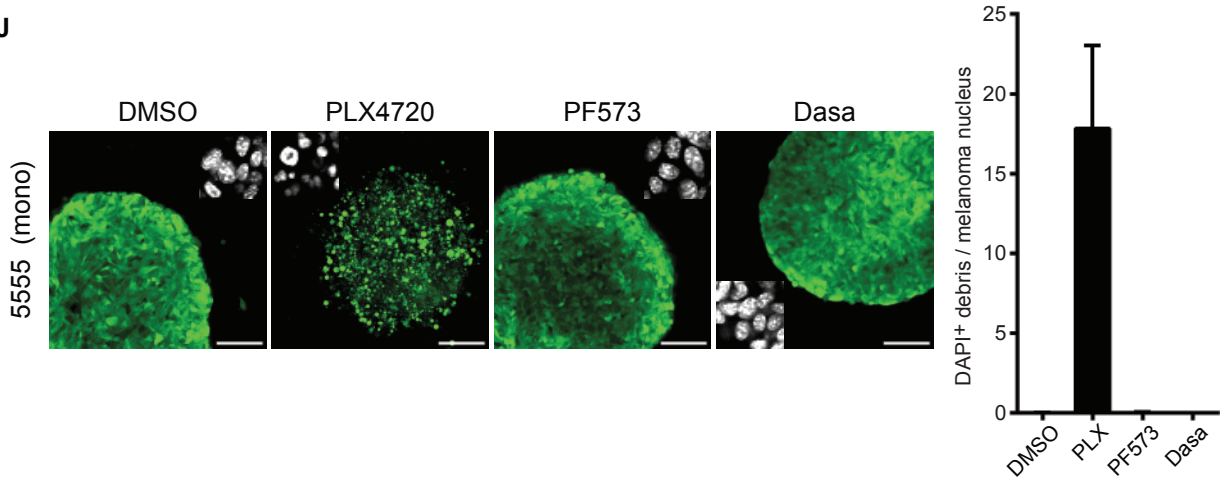
Figure S5. (Related to Figure 5.) Simultaneous inhibition of BRAF and FAK/Src effectively suppresses ERK reactivation in melanoma cells.

(A-F) Images of 5555-EKAREV-NLS and MAF1-mCherry co-cultured spheroids treated with FAKi14 (1 μM), PF562271 (1 μM), PP2 (1 μM), PD184352 (1 μM), imatinib (1 μM) ± PLX4720 (1 μM). ERK activities in imatinib ± PLX4720 treated cells were quantified at the indicated time points and shown in (F) as scatter plots with mean ± SD. Scale bars = 100 μm. (G) Statistical analysis of ERK activity in 5555-EKAREV-NLS and MAF1-mCherry co-cultured spheroids treated with the indicated drug combinations. The values indicate mean ± SD. ND; normalized ERK/MAPK activity 12 hr after addition of indicated drugs, normalized to 30 min before treatment. Red color gradient indicates the effect of the drugs on ERK activity after 12 hr. (H) Images of 4434-EKAREV-NLS and MAF2-mCherry co-cultured spheroids treated with PF573228 (1 μM) ± PLX4720 (1 μM). ERK activities were quantified at the indicated time points and shown as scatter plots with mean ± SD. Scale bars = 100 μm. (I) Statistical analysis of ERK activity in 4434-EKAREV-NLS and MAF2-mCherry co-cultured spheroids, described in the same manner in (G). (J) 5555-mEGFP mono-cultured spheroids were embedded into collagen gels and treated with 0.1% DMSO, PLX4720 (1 μM), PF573228 (1 μM), or dasatinib (200 nM) for 48 hr. Representative DAPI-staining images are also shown in each panel, and the ratio of DAPI-positive debris and melanoma nucleus was calculated and shown as mean ± SD. Scale bars = 100 μm.

Movie S4. (Related to Figure 5.) Simultaneous inhibition of BRAF and FAK/Src abolishes ERK reactivation and effectively induced cell death in 5555 cells.

5555-EKAREV-NLS and MAF1-mCherry co-cultured spheroids were embedded in collagen gels and treated with PF573228 (1 μM) ± PLX4720 (1 μM) or dasatinib (200 nM) ± PLX4720 (1 μM). Images were acquired every 5 min for 13 hr. Scale bars = 100 μm.

A

	A375		WM266.4	
	DMSO	PLX4720	DMSO	PLX4720

ppERK

ERK

pSFK

H&E

Gomori

Fibronectin

B

Integrin β1 (HUTS-21) / DAPI

DMSO

PLX4720

p = 0.0053

p = 0.0158

C

A375-Nu-DMSO
A375-Nu-PLX
WM266.4-Nu-DMSO
WM266.4-Nu-PLX

Cell number (fold change)

Days

D

Add Drugs

- 30 min   + 30 min   + 4 hr   + 12 hr

PLX

PLX + PF

PLX + Dasa

1.5

0.5

PLX   - 30 min
+ 12 hr

PLX + PF   - 30 min
+ 12 hr   p < 0.001

PLX + Dasa   - 30 min
+ 12 hr   p < 0.001

Normalized FRET/CFP

E

Endomucin   αSMA   F4/80   S100A9 (2B10)

DMSO

PLX4720

PF562271

PF562271 + PLX4720
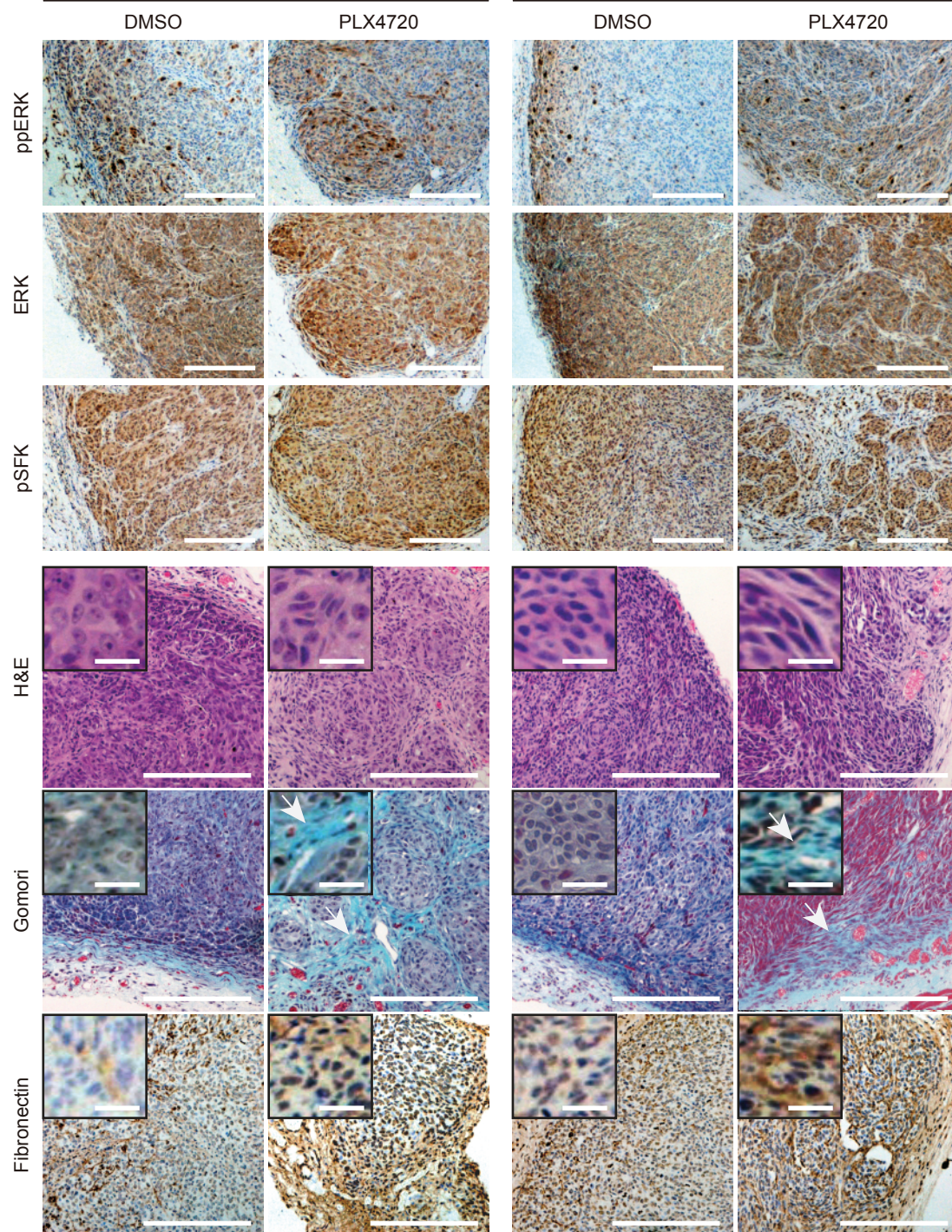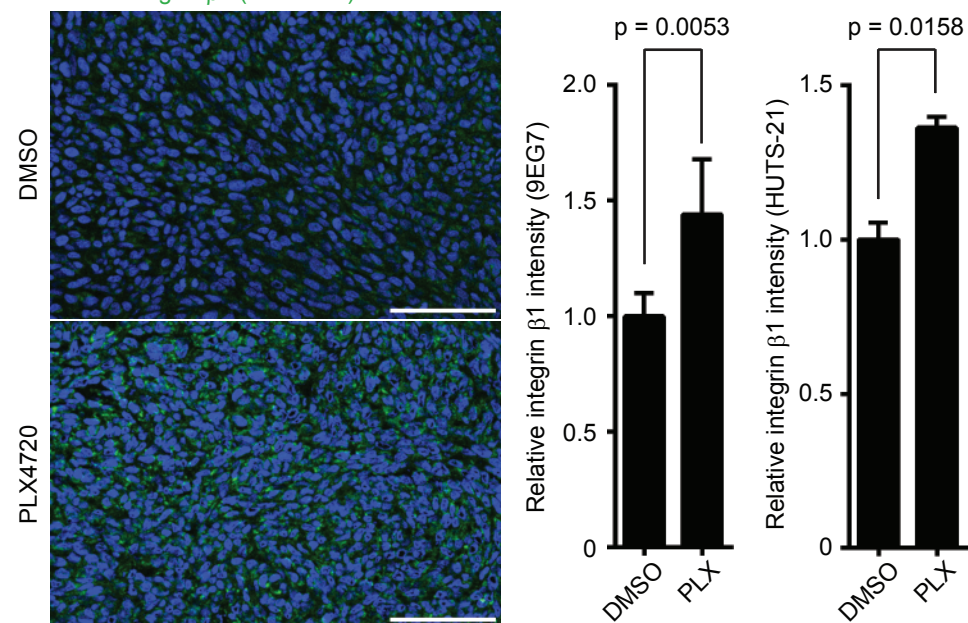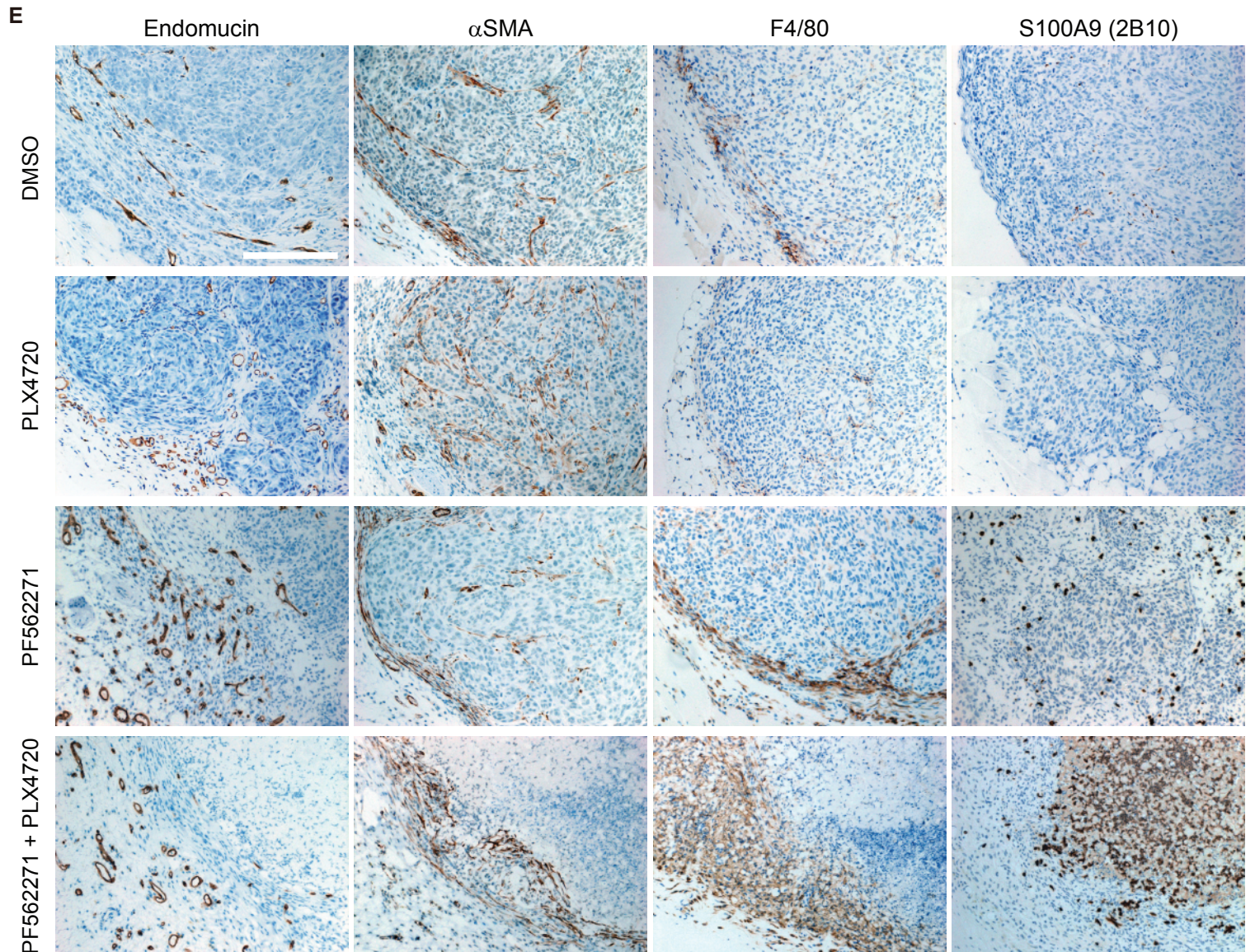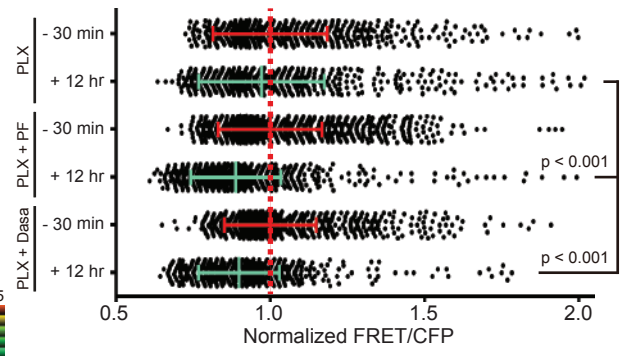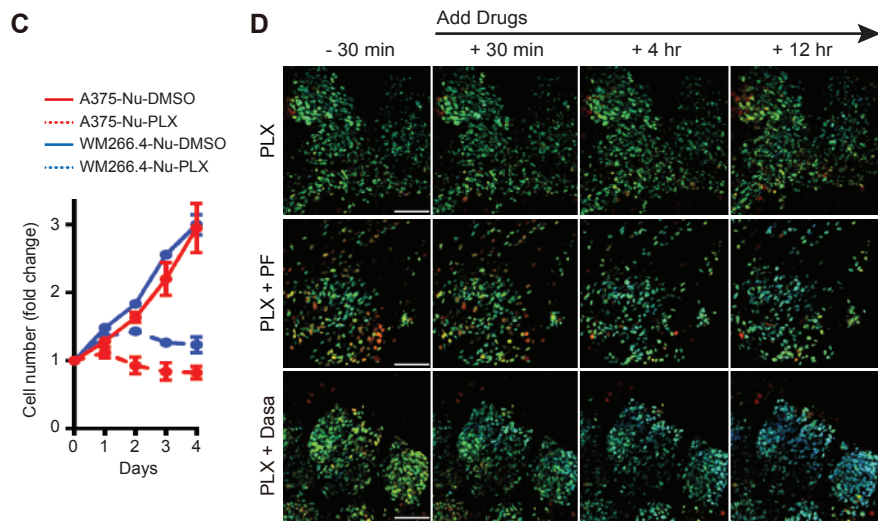
Figure S6. (Related to Figure 6.) GhUV"Y"X]gYUgY"cb"6 F5: "]b\ ]V]hcf "fYUha Ybh]g UggcWUhYX"k]h\ "UhfYX"97 A"UbX"gi ddcfhYX"Vm: 5 ?"g]["bU"]b["

(A) A375 and WM266.4 xenograft tumors grown subcutaneously in nude mice treated with DMSO (4%) or PLX4720 (25 mg/kg) were fixed and stained with the indicated methods/antibodies. Arrows in Gomori trichrome staining indicate thick collagen fibers (bright blue) in PLX4720 treated tumors. Scale bars = 200 μm and 20 μm (insets). (B) Frozen sections of A375 tumors treated with DMSO (4%) or PLX4720 (25 mg/kg) for 15 days were stained with two different anti-integrin β1 antibodies (9EG7 and HUTS-21). Integrin β1 intensities were quantified and shown as mean ± SD. Scale bars = 100 μm. (C) In vitro growth curves of A375 and WM266.4 cells re-established from mouse xenograft treated with PLX4720 (25 mg/kg) for 15 days. Data are represented as mean ± SD. (D) Representative FRET images of A375 explants treated with the indicated drugs in 3D collagen gels. The explants were established from mice treated with PLX4720 for 10-13 days. ERK activities at time -30 min and +12 hr were quantified and normalized to before treatment (-30 min) in each treatment group. At least 6 explants from 2 mice were analyzed in each group and the data are shown as scatter plots with mean ± SD. Scale bars = 100 μm. (E) Immunohistochemical staining with the indicated antibodies of A375 tumors treated with DMSO (4%), PLX4720 (25 mg/kg), PF562271 (50 mg/kg) or the combination for 25 - 29 days. Scale bars = 200 μm.

A

B

Patient #1 (PD, Treat = 1 month)　　　　Patient #4 (PR, PFS = 3 months, Treat = 16 months)

Before　　After prog.　　Before　　After prog.

H&E

Gomori

αSMA

ppERK

pSrc
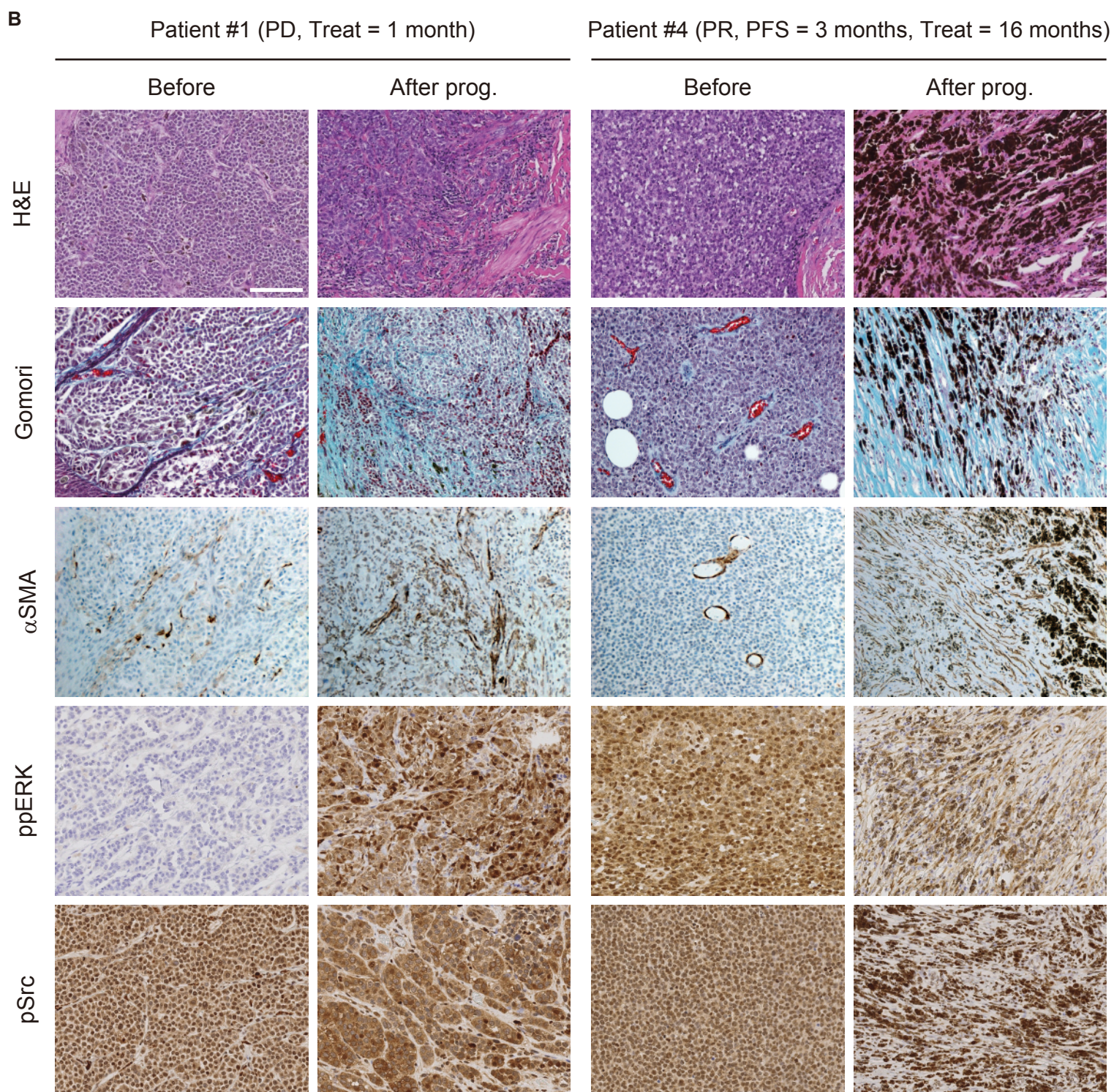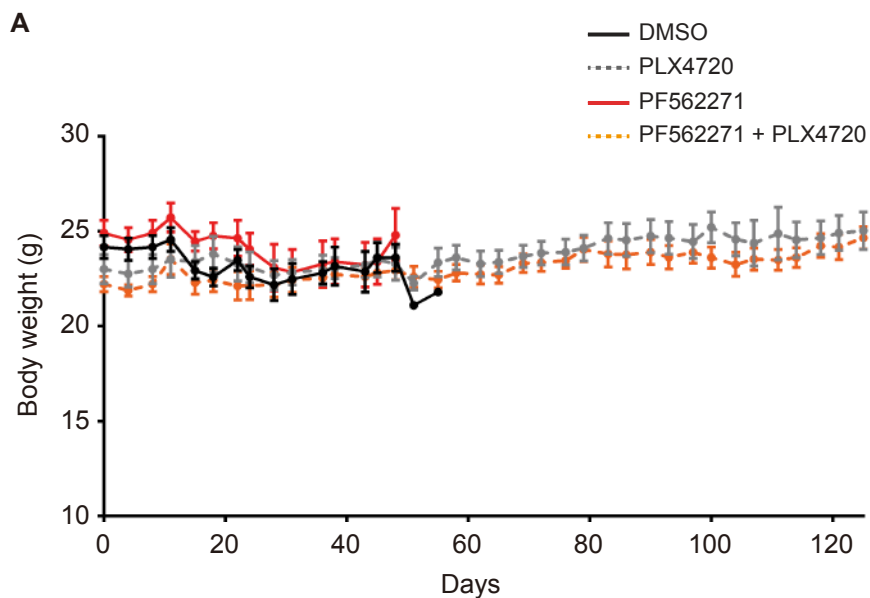
Figure S7. (Related to Figure 7.) Alterations in tumor stroma and ECM in vemurafenib-treated patients.

(A) Body weight curves of PDX-carrying mouse treated with DMSO (4%), PLX4720 (45 mg/kg), PF562271 (50 mg/kg) or the combination. Data are represented as mean ± SEM. (B) H&E, Gomori trichrome, anti-αSMA, anti-phospho-ERK and anti-pSrc staining in paired surgical specimens (before vemurafenib treatment and after progression on drug treatment). Scale bars = 100 μm. PD; progressive disease, PR; partial response, PFS; progression free survival. See also Table S2 for further clinical information. Note: the after progression sample of patient #4 has high levels of melanin (very dark brown), this should not be confused with the lighter brown immuno-staining for alphaSMA, phospho-ERK and phospho-Src.

Table S2. (Related to Figure 7. Provided as an Excel file.) Clinical information of melanoma specimens for a PDX mouse model and histopathological analysis.

SUPPLEMENTAL EXPERIMENTAL PROCEDURES

Isolation and immortalization of human melanoma associated fibroblasts

Melanoma-Associated Fibroblasts (MAFs) were obtained under approval of the UK Research Ethics Committee 08/H0801/129. MAF1 were cultured from a melanoma metastasis behind knee (popliteal fossa met.) removed from a patient at the Royal Marsden Hospital, London. MAF2 were cultured from a melanoma metastasis (BRAF wt) removed from a patient with progressive disease following temozolomide and ipilumimab treatment at the Royal Marsden Hospital, London. Both MAF lines were established with fibroblast purification procedures, as reported previously (Calvo et al., 2013). Briefly, a sample was cut into small pieces and collagenase/dispase digested. After filtering the undigested tissue, the solution was serial centrifuged and the final pellets were re-suspended in DMEM (Invitrogen) with 10%FBS, 1% ITS (Invitrogen) and seeded on a culture dish. After 30 min, fibroblasts have already adhered to the dish while other cellular types remain in suspension. When purified fibroblasts were obtained after repetition of these procedures, cells were immortalized by hTERT introduction with retroviral vectors (Gaggioli et al., 2007).

Longitudinal intravital tumor imaging through an imaging window

All animal experiments were kept in accordance with UK regulations under project licence PPL/80/2368. Surgical procedures for setting up an imaging window was reported previously. 10 Melanoma spheroids (each containing 20,000 cells) were suspended in Matrigel (BD Biosciences) and injected beneath the window set up on the right lower back of C57BL/6 mice. After 5–10 days, the animals were anesthetized and tumor spheroids were imaged longitudinally at the indicated time points with Zeiss 780 inverted microscope.

Tumor explant and spheroid preparation

Tumor explants were prepared by cutting out subcutaneous tumors or experimentally-induced lung metastasis tumors, chopping into pieces (< 1 mm). Melanoma/MAF spheroids (20,000 cells for melanoma spheroids and 10,000 cells each for melanoma/MAF mixed spheroids) were prepared by a droplet culture method as reported elsewhere. Explants/spheroids were embedded in collagen type I gel (BD Biosciences) at a concentration of approximately 4.2 mg/ml and cultured for subsequent experiments.

FRET microscopy and image processing

For epifluorescence FRET microscopy, cells were plated on 35-mm glass-base dishes, maintained in phenol red–free DMEM with 1% FBS and imaged through a 60x oil-immersion objective lens on an Nikon TE2000 microscope (Nikon) equipped with a cooled CCD camera, CoolSNAP HQ (Roper Scientific), and controlled by MetaMorph software (Universal Imaging, West Chester, PA). For the dual-emission ratio imaging of the FRET biosensors, we used a 440AF21 excitation filter, a 455DRLP dichroic mirror, and two emission filters, 480AF30 for CFP and 535AF26 for FRET (Omega Optical, Newton, MA). After background subtraction, the ratio image of FRET to CFP was created with MetaMorph software, and the results were used to represent the FRET efficiency. All ratiometric FRET images are shown in intensity-modulated display (IMD) mode with 32-intensity in 8-ratio, and the gradient of the color bar shows the activity of ERK/MAPK, with higher activity depicted in red and lower activity in blue. For two-photon excitation microscopy (TPEM), animals or samples were kept on a heated stage or in an incubation chamber and imaged through a 20× dry objective lens (Nikon) with an Zeiss 780 inverted microscope equipped with a Laser Diode, an Argon Laser, an HeNe Laser and a Chameleon Ti:sapphire Laser (Coherent Inc.). For two-photon excited FRET imaging, we used the excitation wavelength of 820 nm through an IR-cut filter, MBC760+, and the emission light was separated by beam splitters into 463-506 nm for CFP and 515-559 nm for FRET. Images were acquired as 12-bit images and analyzed with

MetaMorph software as described above, and FRET/CFP in each cell (nucleus) was calculated in a single section using an intensity threshold of 200 A.D.U. for ERK activity quantification. For timelapse FRET imaging of cultured spheroids, images were acquired every 5 min for up to 13 hr (157 serial images), and analyzed in the same manner, but for quantification of FRET/CFP we used a stacked image of 5 sections (4 μm distance each) so as not to miss the information from motile cells. For FRET image presentation, the original images were analyzed with Imaris Software (Bitplane AG, Zürich, Switzerland) and reconstructed into three-dimensional images, or simply presented as maximum-stack images on Metamorph software. The collagen signal was imaged using second harmonic generation in response to an 820 nm pulsed Ti:Sapphire laser. For other fluorescent dye/protein imaging, DAPI was excited with 405 nm, EGFP with 488 nm, and Tomato and Cherry with 561 nm wavelength, using standard beam splitter setting.

ECM-remodeling assay

To assess force-mediated matrix remodeling (Calvo et al., 2013), 25,000 (MAF1) or 50,000 (MAF2) cells were embedded in 100 µL of Collagen I / Matrigel and seeded on a 24-well glass bottom plate. Once the gel was set, cells were maintained DMEM with 10%FBS, 1% PenStrep and 1% ITS. Gel contraction values were measured after 2 days, and the percentage of contraction was calculated using the formula 100 × (well diameter – gel diameter) / well diameter.

TCSPC FLIM-FRET

FLIM experiments were performed successively with the same two-photon microscope used for CFP/FRET imaging. The Ti:sapphire mode-locked laser (80 MHz) was tuned to 820 nm for CFP excitation and CFP fluorescence emissions were collected through a beam splitter, FT455, and a band pass filter, BP480/40 (Zeiss), using a photon counting photomultiplier tube (HPM-100 hybrid PMT, Becker and Hickl GmbH) and a time-correlated single photon counting (TCSPC) module (SPC-

830, Becker and Hickl GmbH). CFP lifetime was analyzed fitting to a triple-exponential decay curve (Becker et at., 2003 and The bh TCSPC Handbook Fourth Edition), and amplitude-weighted mean lifetime was calculated to create a color-scaled lifetime image, ranging from 1.8 ns (red) – 2.4 ns (blue).

Cell proliferation/viability assay

2×10^5 cells in DMEM with 1% FBS were seeded onto 6-well plate and the numbers of the cells were counted by using ViCell Automated Cell Counter (Beckman Coulter) with or without the drugs of interest.

Calculation of DAPI-positive debris/nucleus in spheroid invasion assay

Images were analyzed on Metamorph software. ROIs were set up at the border of spheroids/explants where both the signals from DAPI and GFP (melanoma cells) are detectable. The number of melanoma nucleus was counted manually inside the ROIs, followed by semi-automated counting of DAPI-positive debris: DAPI-staining images are background-subtracted and processed to binary coded > 1000 ADU. 2 ROIs were set in a single spheroid/explant covering the border region, and at least 6 ROIs from 3 different spheroids/explants were analyzed.

Fluorescence-activated cell sorting and microarray analysis.

5555-mEGFP and MAF2-mCherry were co-cultured on 15 cm culture dish with DMSO (0.1%) or LX4720 (1 μM) for 24 hr. Then, cells were trypsinized, re-suspended into PBS with or without PLX4720 (1 μM), and sorted according to the expression of EGFP and Cherry by FACSAria (Becton Dickinson). Cells were directly collected into lysis buffer (RNeasy mini kit, Qiagen) and total RNA was extracted from each fraction. RNA was then processed in collaboration with the Bart's and London Centre for Genome Research (Illumina bead array platform – details available on request). For gene-set enrichment analyses (GSEA), array data was processed and analysed using the Gene-set enrichment analysis software

developed by the Broad Institute of MIT and Harvard (USA) and available at www.broadinstitute.org, following the program guidelines.

ECM screening

96-well glass bottom plates were coated with Collagen I (100mg/ml) +/- Fibronectin (20 mg/ml), CTGF (20 mg/ml), TNC (20 mg/ml), TSP-1 (20 mg/ml), TSP-2 (20 mg/ml), or POSTN (20 mg/ml). 5555/4434 cells stably expressing firefly luciferase were seeded on the plates, cultured overnight. 24 hr after treatment with DMSO or PLX4720, D-Luciferin (150 µg/ml) was added into the wells and the plates were imaged under IVIS Spectrum.

Cell viability assay on PAA/Bis-AA gels with defined stiffness.

PAA/Bis-AA gels with defined rigidity were set up in 12-well glass bottom plates as reported elsewhere. Briefly, 12 µl of solution (see below) was covered with a cover glass and left for 1 hr at RT to set a gel. After removing the cover glass, the gel was coated with 150 µl of Sulfo-SANPAH Photoreactive Crosslinker (Pierce / ThermoScientific) and activated by UV illumination for 10 min, followed by ECM coating. 5555/4434 cells in DMEM were seeded onto the gels, cultured overnight and treated with drugs for 24 hr. Then, cells were stained with propidium iodide (PI, 1mg/ml) and imaged with a Zeiss 780 inverted microscope. For quantification of cell death, PI positive area (> 500 A.D.U.) was divided by the number of surviving melanoma cells. The composition of gels with defined stiffness and ECM concentration are shown below.

Composition of the gels

Young's modulus	0.2 kPa	3 kPa	12 kPa
10mM HEPES	424.7 µl	403 µl	358 µl
40% PAA	37.5 µl	68.6 µl	94.4 µl
2% Bis-AA	7.5 µl	22.48 µl	40 µl
APS	2.5 µl	2.5 µl	2.5 µl
TEMED	0.25 µl	0.25 µl	0.25 µl

ECM concentration

Type of ECM(s)	Coating	Media
Collagen I	Collagen I (100 mg/ml)	
Fibronectin	Fibronectin (20 mg/ml)	Fibronectin (20 mg/ml)
ECM mixture	Fibronectin (20 mg/ml) Tenascin-C (5mg/ml) TSP-1 (5mg/ml) TSP-2 (5mg/ml)	Fibronectin (20 mg/ml) Tenascin-C (5mg/ml) TSP-1 (5mg/ml) TSP-2 (5mg/ml)

Transfection

For DNA transfection to 5555, 4434, C790, B16F10, A375 and WM266.4 cells, we used lipofectamine 2000 (Invitrogen), and for siRNA transfection to 5555 and 4434, we used lipofectamine RNAiMax (Invitorgen), according to the manufacture's protocol. For DNA transfection to MAFs, we used an electroporation system (Amaxa Nucleofector, Lonza AG).

Immunoblotting

Protein lysates were processed following standard procedures (Calvo et al., 2013), and antibody description and working dilutions used can be found in the following section.

HE, Gomori trichrome stain and immunohistochemistry

Hematoxilin&eosin and Gomori trichrome stain were performed as described elsewhere. For immunohistochemical analysis, the conventional avidin–biotin–peroxidase complex method was used as described previously (Calvo et al., 2013). Images were captured using a Nikon TE2000-S equipped with a Nikon DS-5M camera.

Regents, recombinant proteins, siRNAs and antibodies.

Information about reagents, recombinant proteins, antibodies and siRNAs used in this paper are shown below.

<u>Reagents</u>

Reagent	Company	Cat. No
PLX4720	(Made in house)	
	stratech	S1152
	MedKoo Biosciences	202272
PD184352	(Made in house)	
	LC Labs	P-8499
Imatinib	LC Labs	I-5508
Sunitinib	LC Labs	S-8803
PF573228	Tocris	3239
PF562271	MedKoo Biosciences	202228
FAK inhibitor 14	Tocris	3414
Dasatinib	LC Labs	D-3307
PP2	Calbiochem	529573

<u>Recombinant proteins</u>

Protein	Company	Cat. No
Fibronectin	SIGMA	F1141
CTGF	Peprotech	120-19B
Tenascin-C	Millipore	CC065
Thrombospondin-1	R&D systems	P07996
Thrombospondin-2	R&D systems	P35442
Periostin	R&D systems	Q15063

<u>siRNAs</u>

siRNA	Company	Sequence
QIAGEN CTRL	QIAGEN	Not specified (CODE 1027280)
Mouse ITGB1 smart pool	Dharmacon/Thermo Scientific	GAACGGAUUUGAUGAAUGA CCACAGAAGUUUACAUUAA GCACAGAUCCCAAGUUUCA CAAGAGGGCUGAAGAUUAC
Mouse Ptk2 smart pool	Dharmacon/Thermo Scientific	GAACAUGGCCGACCUGAUU GAAGUUGGGUUGUUUGGAA GAAGAUAAGCCAACAUUGA AGAUGUUGGUUUAAAGCGA

Antibodies

Antibody	Company	Cat. No	Dilution		
			IF	WB	IHC
αSMA	Sigma	A2547	1:200		1: 6000
S100A4 (FSP1)	Abcam	ab27957	1:200		
FAP	Abcam	ab53066	1:200		
Fibronectin	Sigma	F3648	1:200	1:1000	1:1000
Ki-67 (clone TEC-3)	DAKO	M7249			1:125
Integrin β1 (HUTS-21)	BD Pharmingen	556084	1:100		
Integrin β1 (9EG7)	BD Pharmingen	550531	1:100		
Integrin β1	Cell Signaling	#4706		1:1000	
phospho-FAK	Cell Signaling	#8556	1:100		
phospho-FAK	Abcam	ab 39967	1:100		
FAK	Cell Signaling	#3285		1:1000	
phospho-ERK	Cell Signaling	#4376		1:1000	1:100
ERK	Cell Signaling	#4695		1:1000	1:100
phospho-MLC	Cell Signaling	#3671		1:1000	
phospho-Src family kinase	Invitrogen	44660G			1:1000
β tubulin	Sigma	T7816		1:200000	
F4/80	Serotec	MCAP497			1:100
S100A9 (2B10)	Abcam	ab105472			1:80
CD3	DAKO	A0452			1:150
CD45R	BD Pharmingen	553086			1:200
Endomucin	Santa cruz	sc-65495			1:100
CTGF	Abcam	ab6992		1:5000	
Tenascin-C	Abcam	ab6393	1:200	1:200	1:4000
Thronbospondin-1	Invitrogen	39-9300	1:100	1:500	
cleaved caspase-3 (Asp175)	R&D systems	MAB835	1:50		

Statistical analysis

Data were subjected to one-way ANOVA analysis, followed by Dunnett's multiple comparison test. When two groups were compared, a two-tailed paired or unpaired Student's *t*-test was applied.

REFERENCES IN SUPPLEMENTAL INFORMATION

Becker, W., Bergmann, A., Biskup, C., Kelbauskas, L., Zimmer, T., Klöcker, N., and Benndorf, K. (2003). High resolution TCSPC lifetime imaging. Proc. SPIE 4963, 1-10.

Becker, W. (2010) The bh TCSPC Handbook Fourth Edition (Becker and Hickl GmbH; http://www.becker-hickl.com)

Gaggioli, C., Hooper, S., Hidalgo-Carcedo, C., Grosse, R., Marshall, J. F., Harrington, K., and Sahai, E. (2007). Fibroblast-led collective invasion of carcinoma cells with differing roles for RhoGTPases in leading and following cells. Nat Cell Biol *9*, 1392-1400.